Characterization of Transgenic Mouse Models for Type V and Atypical type VI Osteogenesis Imperfecta

Samantha Robinson

Department of Human Genetics, Faculty of Medicine and Health Sciences

McGill University

Montréal, Québec, Canada

November 2022

A thesis submitted to McGill University in partial fulfillment of the requirements of the degree of Master of Science

ABSTRACT

Osteogenesis imperfecta (OI) is a rare disorder that causes skeletal fragility, reduced height, and fractures. Two mutations in *BRIL* are known to cause distinct types of OI. A recurrent heterozygous mutation in the 5' UTR (c.-14C>T) is the sole cause of OI type V. This creates a novel in-frame translational start site and results in a 5 amino acid extension (MALEP) on to the N terminus of BRIL (MALEP-BRIL). A missense mutation in exon 1 of *BRIL* (c.119C>T) which changes a serine to leucine at position 40 (S40L) results in a genetically atypical form of OI type VI. This work includes generating and characterizing inducible transgenic mouse models for both types of OI. When either hS40L-BRIL or hMALEP-BRIL were expressed from conception, the skeletal phenotype was extremely severe, causing neonatal lethality. Alizarin red/alcian blue staining showed that long bones were shorter, hypo mineralized, and bowed. The rib cages in both models were wavy, likely the cause of neonatal lethality. RT-qPCR on E18.5 calvaria in both models indicated a significant reduction in the expression of bone-specific differentiation markers (*Bglap*, *Ibsp*, *Col1a1*, and *BRIL*). This indicated a halt in osteoblastogenesis. Primary neonatal calvaria osteoblast cultures from hMALEP-BRIL and hS40L-BRIL showed significant decreases in these differentiation markers when compared to controls. This correlated with decreased mineralization as detected by alizarin red staining. When the hMALEP-BRIL and hS40L-BRIL expression were induced starting postnatally, the mutant mice femur, tibia, vertebrae, and mandible appeared bulky and white. μCT imaging revealed a massive expansion of the periosteal and trabecular compartments in the femur. RNAseq of the 11-week-old tibia and calvaria showed increased expression levels of osteoblast differentiation/activity markers (*Dmp1*, *Sp7, Alpl, Dlx3, Bmp2, Tnfsf11b*). Serum biochemistry analysis showed increased alkaline phosphatase activity, indicating increased osteoblast differentiation and activity. The hS40L-BRIL mice showed a significant decrease (2.8-fold) in blood urea nitrogen. Mice overexpressing the wild-type human BRIL protein were found to be normal at birth, but subsequently display the bone expansion phenotype by 4 to 6 weeks of age. These results point to a unique ability of the human BRIL protein to cause an anabolic effect in mice. Future studies will be necessary to provide clues as to the exact molecular mechanisms causing this phenotype.

RÉSUMÉ

L'ostéogenèse imparfaite (OI) est une maladie rare qui provoque une fragilité du squelette, une taille réduite et des fractures. Deux mutations dans le gène *BRIL* sont connues pour provoquer des types distincts d'OI. Une mutation hétérozygote récurrente dans le 5' UTR (c.-14C>T) est la seule cause d'OI de type V. Cette mutation crée un nouveau site d'initiation de la traduction et entraîne une extension de 5 acides aminés (MALEP) à l'extrémité n-terminale de BRIL (MALEP-BRIL). La deuxième est une mutation ponctuelle dans l'exon 1 de *BRIL* (c.119C>T) qui change une sérine en leucine en position 40 (S40L). Cette mutation cause une forme génétiquement atypique d'OI de type VI. Le présent travail comprend la génération et la caractérisation de modèles de souris transgéniques inductibles pour les deux formes d'OI mentionnées ci-haut. Lorsque hS40L-BRIL ou hMALEP-BRIL sont exprimés dès la conception, le phénotype squelettique est extrêmement sévère, entraînant une létalité néonatale. La coloration au rouge alizarine/bleu alcian a montré que les os longs étaient plus courts, hypominéralisés et courbés. La cage thoracique était extrêmement hypo minéralisée, ce qui est probablement la cause de la létalité. Une analyse par RT-qPCR sur le calvaria des embryons au stade E18.5 a indiqué une réduction significative de l'expression des marqueurs de différenciation spécifiques à l'os (*Bglap*, *Ibsp*, *Col1a1*, *Bril*) dans les deux modèles. Ce résultat suggère un arrêt de l'ostéoblastogenèse. Des cultures primaires d'ostéoblastes de hMALEP-BRIL et hS40L-BRIL ont été isolées afin de déterminer leur potentiel de différenciation et de minéralisation. Ces deux types de cultures ont montré des diminutions significatives des marqueurs de différenciation (*Dmp1*, *Sp7, Alpl, Dlx3, Bmp2, Tnfsf11b*, les mêmes que ceux observé dans le calvaria a E18.5, par rapport aux osteoblastes témoins. Parallèlement, les deux cultures ont montré une diminution du marquage à l'alizarine. Lorsque le hMALEP-BRIL et le hS40L-BRIL ont été exprimé seulement après la naissance, le fémur, le tibia, les vertèbres et la mandibule des souris mutantes semblaient plus volumineux et de couleur blanchâtre. L'imagerie par tomodensitométrie a révélé une expansion massive des compartiments osseux corticaux et trabéculaires. L'immunohistochimie utilisant un anticorps anti-hBRIL a montré une localisation subcellulaire principalement dans les ostéoblastes et certains ostéocytes. L'ARNseq du tibia et du calvaria des souris hS40L-BRIL a montré des niveaux d'expression accrus des marqueurs de différenciation et d'activité des ostéoblastes (*Dmp1*, *Sp7*, *Alpl*, *Dlx3*, *Bmp2*, *Tnfsf11b*). Les deux modèles ont présenté une augmentation significative de l'activité de la phosphatase alcaline à 12

semaines d’âge, un indicateur de l’activité accrue des ostéoblastes et de la formation osseuse. Seules les souris hS40L-BRIL ont montré une diminution significative de 2.8 fois de l'azote uréique sanguin. Les souris exprimant hWT-BRIL de manière constitutive apparaissaient normales à la naissance. Cependant, le même phénotype d'expansion osseuse à l’âge adulte a été observé chez ces souris. Ces résultats suggèrent une capacité unique de la protéine BRIL humaine à provoquer un effet anabolisant chez la souris. Des études ultérieures seront nécessaires pour découvrir d'autres indices sur les mécanismes moléculaires employés par chacune de ces protéines BRIL mutantes qui cause l’OI.

TABLE OF CONTENTS

LIST OF ABBREVIATIONS

Atcb	Gene encoding mouse β-actin
AdipoQ	Gene encoding mouse adiponectin
ALPL	Gene encoding bone-liver alkaline phosphatase
aOI VI	Atypical OI type VI
ANOVA	Analysis of variance
Bglap	Gene encoding mouse bone gamma carboxyglutamate protein
BRIL	Bone-restricted Ifitm-like protein, IFITM5
BRIL	Gene encoding human bone-restricted Ifitm-like protein, *IFITM5*
Bril	Gene encoding mouse bone-restricted Ifitm-like protein, *Ifitm5*
CD81	Cluster of differentiation 81
CD9	Cluster of differentiation 9
cDNA	Complimentary deoxyribonucleic acid
COL1A1	Gene encoding human collagen type 1 α1 chain
Col1a1	Gene encoding mouse collagen type 1 α1 chain
COL1A2	Gene encoding human collagen type 1 α2 chain
CTX-I	C-terminal telopeptides of type I collagen
Cys	Cysteine
DNA	Deoxyribonucleic acid
E	Embryonic day
Fabp4	Gene encoding mouse fatty acid binding protein 4
GFP	Green fluorescent protein
GLI1	GLI family zinc finger 1
GLI2	GLI family zinc finger 2
GLI3	GLI family zinc finger 3
HPC	Hyperplastic callus
IFITM	Interferon induced transmembrane protein
IFITM5	Gene encoding human interferon-induced transmembrane protein 5; aka BRIL
Ifitm5	Gene encoding mouse interferon-induced transmembrane protein 5; aka *Bril*

kDa	Kilodaltons
MALEP	Methionine-alanine-leucine-glutamic acid-proline
MALEP-BRIL	Transgenic bone-restricted IFITM-like with mutant MALEP amino acid extension
MALEP-Bril	RNA transcript of bone-restricted IFITM-like with mutant MALEP amino acid extension encoded by the transgene
MC3T3	Mouse osteoblast precursor cell line
µCT	Micro-computed tomography
Nr4a3	Gene encoding mouse nuclear receptor subfamily 4 group A member 3
OASIS	Old astrocyte specifically induced substance
OI	Osteogenesis imperfecta
OP-CDL	Osteoporosis with calvarial doughnut lesions
P1NP	N-terminal propeptide of type I collagen
PAGE	Polyacrylamide gel electrophoresis
PCR	Polymerase chain reaction
PEDF	Pigment epithelium derived factor
PM	Plasma membrane
Ptgs2	Gene encoding mouse prostaglandin-endoperoxide synthase 2
RNA	Ribonucleic acid
RNase	Ribonuclease
RT-qPCR	Real time quantitative polymerase chain reaction
SERPINF1	Gene encoding human pigment epithelium derived factor
Serpinf1	Gene encoding mouse pigment epithelium derived factor
SGMS2	Human gene for Sphingomyelin synthase 2
Sost	Gene encoding mouse sclerostin
Sp	Specificity protein
Sp7	Gene encoding mouse osterix
UTR	Untranslated region
UMR106	Rat osteosarcoma cell line

LIST OF FIGURES

LIST OF SUPPLEMENTARY FIGURES

LIST OF TABLES

ACKNOWLEDGEMENTS

I would like to acknowledge my supervisor, Dr. Pierre Moffatt for his guidance and mentorship during my studies. His excellence as a scientist is incredibly inspiring. I have appreciated his presence in the laboratory and willingness to discuss results and techniques. I am grateful to have been his student as he has instilled in me the ability to ask research questions and explore the scientific literature. I would also like to acknowledge the members of my supervisory committee, Dr. René St-Arnaud, and Dr. Monzur Murshed for their support, guidance, and suggestions during this project.

I'd like to express my gratitude to the members of the Moffatt laboratory, notably Marie-Hélène Gaumond and Lisa Lamplugh for their willingness to help with laboratory work and teach me the many techniques I am now proficient in and will apply to any future research goals. The other students in the laboratory, Iliana Palenzuela, and Vincent Maranda were helpful, welcoming, and supportive.

I am grateful to the Fonds de Recherche du Quebec- Sante (FRQ-S) and the Research Institute of the McGill University Health Centre (RI-MUHC)for funding and awards. I thank the McGill University Department of Human Genetics and my supervisor for providing me with various opportunities to attend conferences and present my research.

Lastly, I would like to thank my family. My parents, Mark, and Darlene have offered me endless support and encouragement. I owe my accomplishments and success to the resilience and confidence they have taught me.

FORMAT OF THE THESIS

This is a traditional-style thesis prepared in accordance with the guidelines from the Faculty of Graduate and Postdoctoral Studies of McGill University. The thesis consists of 7 chapters. Chapter 1 is the introduction with a background literature review. Chapter 2 is the materials and methods, which explains the methodology used to carry out the experiments discussed in this project. Chapter 3 presents the research findings; Chapter 4 is a discussion of the results and future directions. Chapter 5 is a discussion of the main conclusions. Chapter 6 is the master reference list used to write this thesis. Chapter 7 is supplementary data.

CONTRIBUTION OF AUTHORS

This project was carried out by Samantha Robinson. with help from Marie-Hélène Gaumond, Lisa Lamplugh (senior research assistants) and Pierre Moffatt, PhD. The study was designed by Dr. Pierre Moffatt with contributions from Samantha Robinson. I performed the laboratory experiments: sample collection, skeletal staining, RNA and protein extractions, Rt-qPCR, western blot analysis, cell culture, and μCT analysis. I also performed the data analysis for all the qPCR and μCT data presented in this thesis. Marie-Hélène Gaumond helped to train me in various techniques including RT-qPCR as well as cell culture. Lisa Lamplugh helped with sample processing, bone sectioning and histology.

CHAPTER 1:INTRODUCTION

1.1 Osteogenesis Imperfecta (OI)

1.1.1 Definition and classification of OI

Osteogenesis Imperfecta (OI) is a heritable connective tissue condition characterized by bone (skeletal) deformities, growth deficiency and increased susceptibility to fractures[1]. OI is clinically variable, which formed the basis for the original classification system[2]. The original Sillence classification system for OI was based only on clinical and radiographic findings[2,3]. Most cases of OI are caused by mutations in collagen type I. 85-90% of OI is caused by a mutation in either *COL1A1* or *COL1A2*. The clinical severity of different *COL1A1* and *COL1A2* mutations vary with the collagen chain that is mutated and the location of the mutation. These mutations in collagen type I generally lead to either defective collagen quality, as seen in the more severe type of OI (II, III) or mutations that lead to a decrease in the quantity of collagen (OI type I). OI is now regarded as a collagen-related disorder[1,4]. This means that it can also be caused by defects in collagen folding, posttranslational modification, bone mineralization, and even osteoblast differentiation[1]. The inheritance patten of different OI types includes autosomal dominant and recessive but also X-linked recessive. There are now more than XVIII types of OI that have been classified and several still being classified[1,5,6]. The discovery of all of these genes makes management of patients and therapeutic development complex[1]. A summary of the types of OI and their inheritance pattern is included in Table 1.

Table 1: Types of Osteogenesis Imperfecta (OI) and their inheritance pattern.

OI Type	Gene	Protein	Inheritance
I, II, III, IV	*COL1A1or COL1A2*	Collagen type 1 a1 or Collagen type 1 a2	Autosomal dominant
V, atypical VI	*IFITM5*	BRIL	
VI	*SERPINF1*	PEDF	Autosomal Recessive
VII	*CRTAP*	CRTAP	
VIII	*LEPRE1*	P3H	
IX	*PPIB*	Cyclophilin B	
X	*SERPINH1*	HSP47	
XI	*FKBP10*	FKBP65	
XII	*SP7*	SP7/OSX	
XIII	*BMP1*	BMP1	
XIV	*TMEM38B*	TRIC-B	
XV	*WNT1*	WNT1	
XVI	*CREB3L1*	OASIS	
XVII	*SPARC*	Osteonectin	
XVIII	*FAM46A*	TENT5A	

1.1.2 OI type V (MALEP-BRIL)

Based on the original Sillence classification system mentioned above, patients with OI type IV represented a heterogeneous group of individuals. In 2000, Glorieux *et al*. proposed to categorize a subset into a new class, to be referred to as OI type V based on several commonalities[7]. They all had a dominant inheritance pattern and were negative for mutations in *COL1* genes. Patients with OI type V have an increased incidence of fractures. They also have several defining characteristics such as hyperplastic callus formation after fractures, calcification of the interosseous membrane in the forearm as well as a mesh-like lamellation pattern under polarized light[7,8]. The genetic cause of OI type V is a recurrent heterozygous mutation in the 5'-untranslated region (UTR) of *IFITM5* (Interferon inducible transmembrane protein-5), also known as *BRIL* (Bone restricted Ifitm like)[8,9]. The point mutation (c.-14C>T) creates a novel in-

frame translation start codon that adds a five amino acid extension (methionine - alanine - leucine - glutamic acid - proline (MALEP)) onto the (N)-terminus of BRIL, creating a mutant protein (henceforth referred to as MALEP-BRIL)[8].

Although genotypically OI type V is homogeneous, the clinical phenotype is variable[10,11]. There have been about 200 cases of OI type V reported worldwide in the literature, affecting many different ethnicities. Rauch *et al* concluded that the phenotypic variability between all the patients they saw with the same mutation was considerable[10]. Zhytnik *et al* also published that the phenotype OI type V patients ranged from mild to extremely severe. This study analyzed 90 unrelated OI patients and identified four patients (4.44%) with OI type V[12]. Three patients came from the Ukrainian OI cohort and one from the Vietnamese cohort. The craniofacial features in OI type V have been studied. One study reported that OI type V is associated with multiple missing permanent teeth, especially premolars. Type V OI is not associated with dentinogenesis imperfecta or blue sclera[13]. This pattern of craniofacial abnormalities is distinct from other severe OI types[13]. A recent study investigated 13 individuals from seven Chinese families with confirmed OI type V[11]. They report significant clinical variability, even within families[11]. They investigated the process of hypertrophic callus formation and measured increased erythrocyte sedimentation rate and levels of C-reactive protein in patients with hyperplastic callus formation[11]. This suggested that inflammatory activation could be involved. Analysis of bone samples from patients with OI type V indicated expression of both the *MALEP-BRIL* transcript and production of MALEP-BRIL protein[14]. This confirmed that the MALEP-BRIL protein is being produced and leads to hypothesis that the resulting OI phenotype is due to a gain of an aberrant function of this mutant protein, not haploinsufficiency. The mechanism by which the MALEP-BRIL causes OI type V, however, is still unknown.

1.1.3 Atypical OI type VI (S40L-BRIL)

Another mutation in *BRIL* was discovered which results in a rare form of severe OI[15-18]. The mutation is a heterozygous (dominant) missense mutation in exon 1 of *BRIL* (c. 119C>T; p. Ser40>Leu)[15,16]. The mutated serine (Ser) at position 40 is a highly conserved residue of BRIL. None of the classical features seen in the OI type V patients were observed[15,16]. Patients were at first thought to have OI type VI based on histological findings of unmineralized osteoid and a fish scale pattern under polarized light in iliac bone biopsies[15]. These histological findings were more consistent with OI type VI[19]. Homozygous mutations in *SERPINF1*, encoding for PEDF (pigment epithelium derived factor) are the genetic cause of OI type VI[1,20]. However, the patient was found to have no mutations in *SERPINF1* and had serum PEDF levels in the normal range[15]. The Ser40>Leu mutation in *BRIL* was therefore referred to as atypical OI type VI (aOI VI). A number of recessive mutations *SERPINF1* have been reported in the literature[20]. Patients with OI type VI have a unique phenotype. They do not have fractures at birth, but they progressively have more fractures leading to deformities. They all have vertebral compression and growth restriction is moderately severe[15,21]. PEDF is a secreted protein with multiple known functions. It is a potent anti-angiogenic factor that inhibits tumor growth, an anti-apoptotic factor and has even been implicated in lipid metabolism[15,22-24]. OI type VI patients have undetectable serum PEDF levels (less than 0.3 mg/L)[15,25]. In contrast, normal PEDF values are reported in type V OI, as well as in OI caused by collagen defects (I-IV)[25].

Culturing of primary osteoblast cells from a patient with the Ser40>Leu BRIL mutation led to a few key findings. Farber et al. reported a decrease in expression in various osteoblast genes; including *COL1A1*, *BGLAP* (gene encoding osteocalcin) and *SERPINF1*. This decrease in *SERPINF1* expression and concomitant decrease in secreted PEDF by the patient osteoblasts led

to the hypothesis of a link between BRIL and PEDF[15]. The authors hypothesized that the poor bone and mineralization phenotype observed in their proband may have arisen from decreased bone-specific expression of PEDF. The mechanism of how a point mutation in BRIL results in severe OI, distinct from OI type V, still remains to be ascertained.

1.1.4 Newly discovered mutations in *BRIL*

Recently, besides the above-described MALEP and S40L variants, there have been additional mutations discovered in *BRIL*. First, a Ser40Trp variant was found in a proband who presented with multiple fractures in utero, but then remained fracture free afterwards except for those related to trauma[18]. This patient showed progressive lower limb deformity but was able to walk independently without additional fractures until 10 years of age. Second, Mäkitie *et al.* described a Japanese family with the skeletal phenotype of osteoporosis with calvarial doughnut lesions (OP-CDL)[26]. The affected individuals with OP-CDL normally have moderately severe OI characterized by childhood-onset skeletal fragility with multiple long-bone fractures, scoliosis and bone deformities[26]. The genetic cause of OP-CDL was identified as mutations in sphingomyelin synthase 2 (*SGMS2*)[26]. In this patient's case, however, whole-exome sequencing identified a novel *BRIL* missense mutation (p.N48S)[26]. The authors acknowledge the limitations of this study only being in one family as well as the lack of functional assessment of the molecular outcomes of the identified mutation. Lastly, another heterozygote variant was identified in the 5'UTR of *BRIL* at position -9 (c.-9C>A)[27]. This base change leads to a novel ATG translation start site and the addition of 3 amino acids (MET-GLU-PRO) in frame with the natural coding of BRIL. Clinically, the newborn proband only manifested a rare clavicle transection fracture with delayed early healing, but no other OI features, making it difficult to

fully correlate the genotype-phenotype in this case. Altogether, these patient findings indicate a need for studies to delineate the molecular mechanisms by which each of these alterations in *BRIL* are leading to distinct phenotypes.

1.1.5 BRIL is part of the IFITM (Interferon induced transmembrane) protein family

In 2008, Moffatt *et al.* screened a UMR106 rat osteosarcoma cell line library and identified a small transmembrane protein which they called BRIL (bone-restricted Ifitm-like)[28]. The gene encoding BRIL had previously been identified by in silico approaches as *Ifitm5* based on gene location and exon structure[28]. Osteoblast cultures were generated to monitor *Bril* gene expression over time. This was to determine what stage during osteoblastogenesis that *Bril* was expressed. In all cultures, *Bril* increased with differentiation and mineralization. In MC3T3 (mouse osteoblast) cells treated to differentiate, *Bril* expression began to be detected at D7 and increased until D21[28,29]. No expression of *Bril* was observed in other bone related cells, such as mouse osteocyte or osteoclast cultures[28]. This data strongly indicates that BRIL is osteoblast-specific. Bril is also considered an osteoblast cell marker, as it is detected once the cells are differentiating and beginning to mineralize. Given it's highly specific expression, its name was changed from *IFITM5* to *BRIL* (Bone Restricted Ifitm like)[28].

BRIL is part of the IFITM (interferon-inducible transmembrane protein) family. The IFITM genes are clustered on the mouse and human chromosomes 7 and 11, respectively. The family members share the same structure, two coding exons separated by a small intron. Mouse members include *Ifitm1*, *Ifitm2*, *Ifitm3*, *Ifitm5* (*Bril*), *Ifitm6* and *Ifitm10*[30]. *IFITM1-3* contain interferon (IFN) response elements within their promoter regions, resulting in them being inducible by IFN-α[30,31]. Although presenting some homologies in terms of sequence and gene

location, *BRIL* is unique from the other IFITM family because it is not responsive transcriptionally by interferons, and its expression is highly cell-specific in osteoblasts[32]. These unique characteristics of *BRIL* are what make it important to study in the context of bone biology. Expression timing of *Bril* is unique being first noted at E14.5, while that of *Ifitm1-3* has been detected in mice as early as E5.5. IFITM1-3 are all ubiquitously expressed proteins and have been found to be involved in various physiological roles such as cell adhesion, apoptosis, tumour progression and more. Additionally, one of the most ascribed and critical functions of IFITM1-3 is as antiviral proteins due to their induction in response to viral infection[33]. In fact, IFITM1-3 impart cellular resistance against a variety of viral pathogens which include Ebola, influenza A, West Nile, Dengue virus, and HIV-1[34-36]. No antiviral function has been reported for BRIL. At the protein level, there are significant sequence differences between BRIL and other IFITMs. The similarity between the mouse IFITM protein family members is observed by comparing the similarity of the protein sequence. BRIL is only 52% similar to IFITM1, 48% similar to IFITM2 and 53% similar to IFITM3[28]. The protein sequence similarity between the other members is much higher (between IFITM1, IFITM2 and IFITM3) it is close to 90%[28]. The alignment of BRIL with the other IFITM family members is shown in Figure 1 below. This shows that BRIL diverges more from the IFITM family members than they do amongst themselves. This suggests a unique role for BRIL, which is in osteoblast cells.

When compared between species, the BRIL protein sequence is highly conserved. For example, an overall 88% similarity is observed between mouse and human protein sequences[28]. There is a 96% similarity between mouse and rat BRIL protein sequences[28]. The total molecular mass is 14.9 kilodaltons (kDa). The number of amino acids (AA) varies from 131 to 134. Human BRIL protein consists of 132 AA residues and mouse BRIL consists of 134 AA residues[28]. The

protein sequence alignment of BRIL across species is presented in Figure 2. This evolutionary conservation underscores the importance of BRIL.

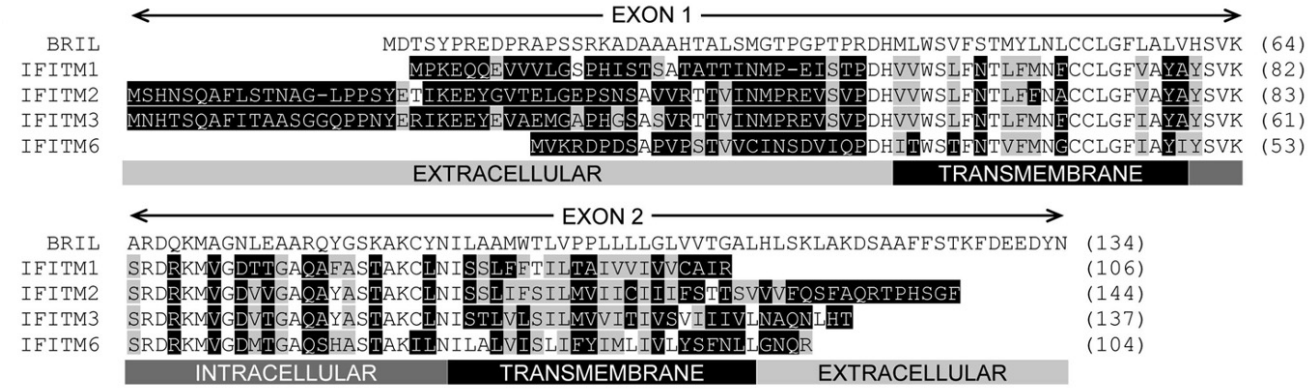

Figure 1: Homology of IFITM protein family members.

Ifitm family members are composed of two exons (black pointed arrows). Protein sequence alignment of mouse IFITM protein family members. Black shading indicates non-identical residues and gray shading indicates conserved residues compared to BRIL (IFITM5). This figure was adapted from a manuscript by Moffatt *et al*[28].

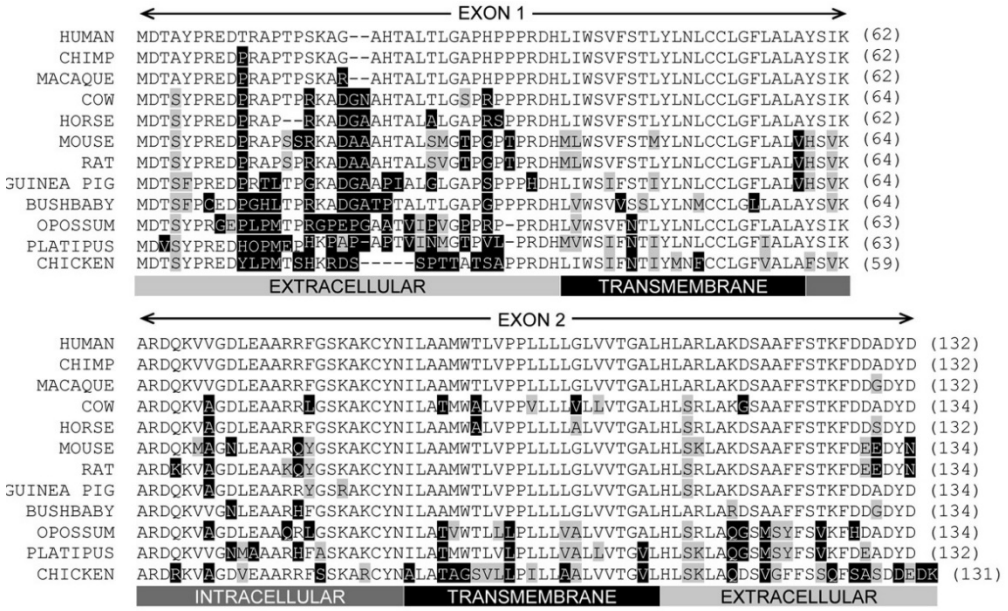

Figure 2: Protein sequence alignment for BRIL in various species.

Amino acid sequences for BRIL were aligned utilizing data from Ensembl release 48. Black shading indicates non-identical residues and gray shading indicates conservative residues with respect to the human sequence. Figure was adapted from manuscript by Moffatt *et al*[28].

1.1.6 Regulation of *BRIL* expression

Our laboratory studied the transcriptional regulation of *Bril* expression in osteoblasts to determine how it was controlled in the human, rat, and mouse gene promoters. Kasaai *et al* used luciferase reporter assays in UMR106 osteosarcoma cells and determined that most of the base-line regulatory activity was localized within 250 bp upstream of the coding ATG of *Bril*[37]. One mechanism for positive modulation of *Bril/BRIL* transcription is through the specificity protein (Sp)-family of transcription factors (TF). The human, rat, and mouse promoter regions of *BRIL* contain many Sp1-like, GC-rich binding sites for TF attachment. Both *Sp1* and *Sp3* were found to be strong inducers of the *Bril* promoter activity[37], in addition to osterix (Sp7)[37]. The positive effects on transcription of *Bril/BRIL* are most pronounced when all three TFs were combined, resulting in a synergistic effect[37]. In addition to Sp binding sites, GLI2 was found to be a powerful positive modulator of *Bril*, whereby the promoter region contains a single canonical binding site[37]. GLI TF (GLI1, GLI2, and GLI3) are regulated by the hedgehog signaling pathway. Binding of hedgehog to Patched releases inhibition of Smoothened[38]. This activates downstream modifications in expression of various genes via GLI TF effects[38]. The *BRIL* promoter was most responsive to GLI2; but family members GLI3 and GLI1 can also mildly increase transcription[37]. It was also found that Indian hedgehog, a secreted molecule that regulates osteoblastogenesis, could potently induce expression of BRIL in culture.

In addition to regulation through binding of TF to the promoter region of *BRIL*, that same study revealed that CpG methylation of this region was also found to be important for adequate expression. In proliferating MC3T3 osteoblasts, which do not express *Bril*, all possible CpG dinucleotides in the promoter region and first exon were methylated, whereas in differentiating

cells, demethylation was observed coinciding with onset of *Bril* expression[37]. Therefore, transcription of *Bril/BRIL* appears to be dependent on CpG demethylation of the promoter[37]. This observation bears relevance to the c.-14C>T (MALEP-BRIL) mutation as this site falls exactly within a CpG dinucleotide that is prone to mutation by cytidine deamination (C>T) during the process of methylation/demethylation[39].

1.1.7 Topological mapping and sub-cellular localization of BRIL

From the original characterization of BRIL, immunolocalization experiments indicated that the protein was in a type III orientation regarding its transmembrane conformation. This orientation suggested that both the N- and C-termini of BRIL were in the extracellular space and that the BRIL protein was crossing the plasma membrane twice via two transmembrane passages[28]. This type III topology was also long thought to be the conformation for other IFITM protein family members. Recent re-evaluations of IFITM topological conformations have suggested a type II protein orientation, with a cytoplasmic N-terminus and an extracellular C-terminus, for IFITM1 and IFITM3[40,41]. Re-evaluation of the BRIL transmembrane topology in our lab indicated a type II conformation[32]. Detection of BRIL N-terminus was only possible after cell permeabilization and trypsinization of live cells expressing BRIL only cleaved off the C-terminus, confirming that it is a type II protein[32]. This BRIL type II topology at the plasma membrane is illustrated in Figure 3.

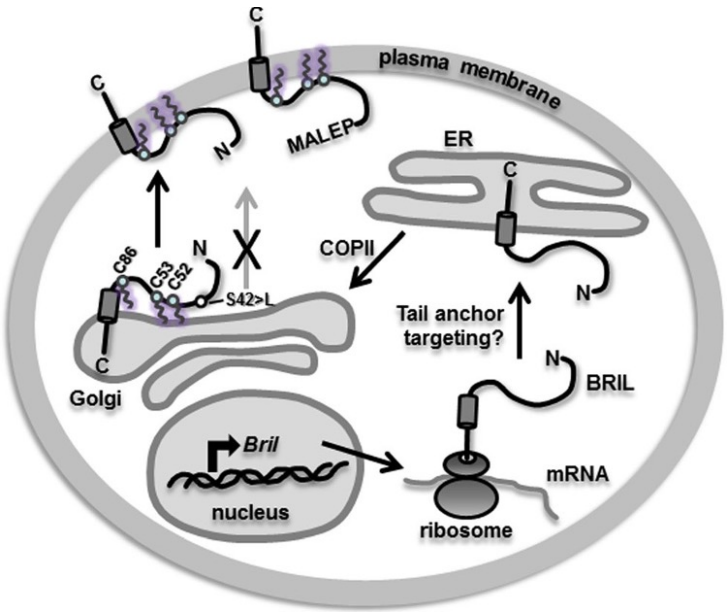

Figure 3: Topology of BRIL at the plasma membrane.

This figure presents a schematic image of the hBRIL protein at the plasma membrane. BRIL is a type II membrane protein that is palmitoylated. BRIL contains a cytoplasmic N-terminus (N), a single transmembrane domain (cylinder), and an extracellular/luminal C-terminal tail (C). After translation, BRIL is targeted to the endoplasmic reticulum (ER). Trafficking of BRIL from the ER to the Golgi is COPII-vesicle dependent. The OI type V BRIL mutant (MALEP-BRIL) is also localized at the cell surface, but not the S42 > L which is trapped in the Golgi). This figure is being used as a summary of the topology discovered for the BRIL protein and is an adapted figure from a manuscript by Patoine *et a*l from our laboratory[32].

It has been established that in osteoblasts, the majority of BRIL protein is localized at the plasma membrane and in the Golgi[32]. Proper plasma membrane targeting and intracellular trafficking of BRIL is dependent on certain cysteine residues and their modifications by palmytoylation[32]. Palmitoylation is a post-translational modification that adds 16-carbon lipid palmitic acid molecules covalently linked by thioester bonds to Cys residues (S-palmitoylation). This modification is reversible and can have different purposes such as to promote membrane association and attachment as well as contribute to molecular interactions[42]. BRIL contains three

cysteine (Cys) residues that are conserved across all species. In vitro analysis indicated that all Cys residues were palmitoylated, but only Cys52 and/or Cys53 were necessary for the proper membrane targeting of BRIL. Mutation of mouse BRIL residues Cys52 or Cys53, but not Cys86, significantly reduced localization of the protein at the plasma membrane and it is instead trapped in the ER-Golgi network. This underscores the importance of this biochemical posttranslational modification on localization of BRIL[32,43]. Furthermore, this could affect any interactions in an indirect manner[32,43]. It was reported that association of BRIL with the ER-associated protein (FKBP19), was dependent on the adequate palmitoylation[44]. Mass spectrometry analysis suggested that FK506-binding protein (FKBP)-19 (encoded by FKBP11) was an interaction partner for BRIL[44] in vitro using MC3T3 osteoblasts . Investigation of the interaction of BRIL with FKBP19 identified a potential further more complex protein association. Hanagata & Li concluded from various assays that osteoblasts formed a FKBP19-CD81-CD9 complex[44]. When BRIL associates with FKBP19 and/or CD8, CD9 dissociates and downstream modifications occur[44]. The significance of the FKBP19- BRIL interaction is still unclear as our laboratory has not been able to reproduce these results using a yeast-2-hybrid approach[45]. It appears that other structural elements within the BRIL polypeptide also contribute to its plasma membrane localization. Indeed, our group has confirmed that the mouse S42L-BRIL (equivalent to the human S40L) protein is unable to localize at the plasma membrane and is trapped in the ER-Golgi[32]. The S40 residue lies in a region that is conserved amongst other IFITM protein members and that was predicted to form an amphipathic helix[32]. It has not been formally interrogated whether this is true for BRIL. This information makes this mutation unique and led to our hypothesis that OI type V and atypical type VI are caused by distinct mechanisms and that ER-related stress could be involved in atypical OI type VI.

1.2 Delineating the physiological role of BRIL in vivo

Several laboratories, including ours, have generated different genetically modified mouse models to better characterize the *in vivo* role of *Bril/BRIL* as well as the mechanisms by which mutant *Bril* would lead to the skeletal phenotypes seen in OI type V and atypical OI type VI. The main characteristics of these mouse models are presented below.

1.2.1 Bril knockout mice

A global *Bril* knockout mouse was generated by Hanagata *et al*. by deleting both *Bril* exons. They reported a mild skeletal phenotype. They stated that the long bones of their homozygous mutants (Ifitm5$^{-/-}$) were shorter than those of the heterozygotes[46]. However, they did not report any significant differences in bone morphometric parameters. *Ifitm5* deficiency did not affect osteoclastogenesis nor osteoblastogenesis[46]. They also reported issues with reproduction (smaller litters from homozygotes)[46]. Our laboratory generated a BRIL knock-out/LacZ knock-in model[47]. Global inactivation of *Bril* was confirmed and a thorough analysis of the skeletal phenotype of the resulting mice was conducted. Embryonic time points spanning from E13.5-E18.5 were studied. These embryos showed significant X-Gal staining without any patterning abnormalities[47]. In the post-natal mice, there was no obvious skeletal phenotype and no bone deformities observed at any time point[47]. There were transient very minor differences noted in terms of bone length and uCT parameters, but not y across all ages and sexes[47]. These changes never resulted in significant alteration in bone material properties and no changes were detected in circulating serum markers of bone turnover (P1NP, CTX-I). Overall, the *Bril* knock-out mice grew and reproduced completely normally (up to 12 months)[47]. This demonstrated that *Bril* is dispensable for proper bone development[47].

1.2.2 Transgenic overexpression of *Bril*

Lietman *et al* developed transgenic mice overexpressing either the wild type mouse BRIL or the MALEP-BRIL (type V) under the control of an osteoblast-specific *Col1a1* 2.3-kb promoter[48]. The transgenic mice showed completely normal growth and development[48]. This indicated that overexpression of wild type *Bril* did not negatively impact bone development or growth. In that same study, transgenic mice constitutively overexpressing the mouse MALEP-BRIL were never generated as carriers of the transgene were always found dead at birth. The E15.5 and E18.5 transgenic MALEP-BRIL embryos had abnormal mineralization and skeletal defects, including a hypo mineralized rib cage and long bone deformities[48]. Primary osteoblast cultures from E18.5 embryos showed decreased mineralization. Expression of osteoblast differentiation markers were reduced[48].

Using the CRISPR-Cas9 technology, our laboratory generated a knockin (KI) mouse model with the exact genetic mutation (c.-14C>T) causing OI type V[49]. Unfortunately, no live descendants were obtained from the mosaic founder animals[49]. All affected pups were found dead at birth. Whole body skeletal staining with alizarin red/alcian blue and μCT imaging of KI embryos also revealed extreme hypo mineralization affecting the skull, bent long bones with little mineralization, and wavy ribs[49]. The midshaft of long bones was filled with hypertrophic chondrocytes[49]. Gene expression analysis at E15.5 and E17.5 showed decreased expression of *Bril* itself but also other important osteoblast differentiation markers (*Ibsp*, *Bglap*, *Sost*). This indicated an overall decrease in osteoblastogenesis and thus mineralization. In contrast, other genes (*Ptgs2, Msmp, Nr4a3)* were found to be upregulated. These have been previously related to an inflammatory signature, and suggested that a pro-inflammatory response was initiated in

the OI type V mice. Overall, these studies do show that the OI type V mutation causes a halt in the differentiation of osteoblasts and a decrease in mineralization[49]. Unfortunately, the use of this model was limited to study the mechanisms occurring during embryogenesis but not in the post-natal period[49]. In order to reflect the disease progression seen in the patients over time and potentially to test therapeutics, it would be advantageous to have a model that could be studied during growth and development[49]. Mechanistically, this study suggests a possible mechanism including a shift of progenitor cells towards adipocytes and an activation of an inflammatory response[49].

Hanagata *et al.* also employed CRISPR-Cas9-based technology to generate mosaic c.-14C>T mutant mice[50]. They reported that mice with less than 40% mosaicism did survive, but did not present with skeletal anomalies. Mice with more than 40% mosaicism were found to have lethal skeletal abnormalities[50]. All the resulting heterozygous pups for the mutation after breeding were found to be perinatal lethal[50]. They also studied the effects of immunosuppressants (FK506) on their model, with the hope that it could improve survival. Administration of FK506 (a calcineurin inhibitor) in the heterozygous fetuses slightly improved bone mineral content of the neonates but did not prevent neonatal lethality[51].

An *in vitro* study recently published by our laboratory used a luciferase reporter assay to screen which of 26 transcription factors could be activated by expressing MALEP-BRIL in MC3T3-E1 and MLO-A5 cells[45]. This study was conducted to explore the concept that the MALEP-BRIL would cause a gain of function. When overexpressed in MC3T3-E1 and MLO-A5 cells, MALEP BRIL activated the reporters dependent on MEF2, NFATc, and NR4A[45]. Additional co-transfection experiments with MEF2C and NFATc1 and several of their

modulators (HDAC4, calcineurin, RCAN, FK506) indicated additive or synergistic activation of these pathways by MALEP-BRIL[45]. Interestingly, the increased *Ptgs2* gene expression was previously shown to be a direct target of transcriptional activation by MEF2 and NFATc.

Very recently, a model for atypical type VI OI was generated[52]. Hedjazi *et al* generated and characterized a novel heterozygous BRIL p.S42L knock-in mouse model, which is the equivalent of the human S40L mutation. They reported that BRIL p.S42L female mice are viable and do not differ in body size, fat or lean mass from wild type mice. However, they observed that the homozygote p.S42L mice had lower whole-body, lumbar and femoral bone mineral density (BMD) and multiple fractures[52]. The p.S42L mice displayed bone tissue abnormalities associated with OI. These included hypermineralization of the matrix, elevated cortical porosity, increased osteocyte lacunae density, and highly disordered collagen fibrils. Therefore, the authors concluded that these OI-related bone tissue alterations were likely to cause overall skeletal fragility[52].

1.3 PROJECT RATIONALE AND OBJECTIVES

This project builds on the knowledge that has been acquired through previous mouse models. Since *BRIL* knockout mouse models have demonstrated that BRIL is dispensable for bone growth and development, it is hypothesized that the two mutant forms of BRIL lead to OI via a gain of an aberrant function[47]. We hypothesized that the MALEP-BRIL and S40L-BRIL were likely acting via different mechanisms based on their palmitoylation status and their subsequent cellular localization. This was not observed for MALEP-BRIL which is localized normally at the plasma membrane. The mechanisms by which the mutant proteins cause these distinct forms of OI is still yet to be ascertained.

The primary goal of this project was to characterize the phenotypes of mouse models that overexpress the human BRIL proteins, MALEP-BRIL and S40L-BRIL. These were generated as conditional transgenic models, based on the TET-OFF system, whereby the transgene expression can be regulated (turned 'on' or 'off') in a temporo-spatial manner by administration of the antibiotic doxycycline. This would allow us to bypass any potential neonatal lethality and analyze the phenotypes at post-natal ages.

The secondary goal of this project was to potentially study the *in vivo* role of *BRIL* and to delineate the mechanism by which the MALEP-BRIL and S40L- BRIL lead to the onset of OI type V and atypical type VI respectively.

CHAPTER 2:MATERIALS AND METHODS

2.1 Generation of inducible transgenic mouse models

The transgenic construct used for all mouse models in this report is shown in Figure 3 below in the results section. The transgenic construct was injected into B6C3F1 egg donors at the Institut de Recherches Cliniques de Montréal (IRCM). Founder lines were established and analyzed. There were three founder lines from each model that transmitted the gene to offspring and were thus maintained and characterized in the laboratory. Animal procedures were reviewed and approved by the Shriners Animal Care Committee and followed the guidelines of the Canadian Council of Animal Care. The resulting transgenic mice were bred with an established transgenic mouse harbouring the tTA in the transgene. The Osx-tTA-GFP:Cre mouse was used for the majority of our studies including those in this report[53]. The Col1a1-tTA transgene was also used to validate the post-natal phenotype and yielded the same results[54].

2.2 PCR genotyping of transgenic mice

Genotyping was performed using PCR amplification on gDNA prepared from mouse tail or mouse ear clipping samples. Samples were digested overnight rotating at 55℃ in lysis buffer (0.1 mM Tris (pH 8), 0.2 M sodium chloride (NaCl), 5 mM ethylenediaminetetraacetic acid (EDTA), 0.4% sodium dodecyl sulfate (SDS)) with 250 µg proteinase K added. DNA was precipitated using isopropanol, washed with 70% ethanol, dried and then resuspended in Tris-EDTA buffer (10 mM Tris (pH 8) and 0.1 mM EDTA).

The PCR mix was prepared using 1x standard Taq buffer, 5 mM dNTP mix and Taq DNA polymerase (New England Biosystems) with 12.5 μM of each primer (Fwd+Rev). The PCR products were resolved on a 1.5% agarose gel to determine the genotype. To determine if tTA was present, primers for Osx-Cre transgene were used with the same PCR protocol. Primers used are in Table 2.

Table 2: List of primers utilized to genotype transgenic mice.

Name	**Sequence (5' > 3')**	**Strand**	**Purpose**
hBRIL F2	CCCACACAGCCCTCACACTG	Forward	Transgene genotyping
hBRIL R2	CGGCACCAGCGTCCACATC	Reverse	Transgene genotyping
Cre_AA_Fwd	GCCTGCATTACCGGTCGATGCAACGA	Forward	Osx-Cre genotyping
Cre_AA_Rev	GTGGCAGATGGCGCGGCAACACCATT	Reverse	Osx-Cre genotyping
h-m-Bril-F1	CAAGTGCTACAACATCCTGGC	Forward	*Bril/BRIL* from the transgene
SV40-pA-R3	GGTATGGCTGATTATGATCCTC	Reverse	*Bril/BRIL* from the transgene

2.3 Collection of tissue samples for embryos and newborns

Newborn male and female mice of all genotypes (WT, tTA^+, Tg^+, and $Tg^+;tTA^+$) for all transgenic models were collected at the embryonic and newborn stages. All animals that did not carry both BRIL and tTA transgenes (Tg+;tTA+) were collectively used as 'control' littermates. The calvaria was dissected of soft tissue and stored in RNAlater solution (Ambion) at -20°C until

processing. The remainder of the skeleton was processed for whole skeleton staining with alizarin red/alcian blue (section 2.3).

2.4 Whole skeleton staining with alizarin red and alcian blue

Embryos at a chosen developmental stage (E18.5) as well as newborn pups were processed for the whole skeleton staining with alizarin red (bone) and alcian blue (cartilage) according to published standard procedures[55].

2.5 Cryo-sectioning of embryos or newborns

Limbs (arm and/or leg) were fixed in 4% PFA and then incubated in 20% sucrose for 24 hours at 4°C followed by 24 hours in 1:1 20% sucrose:OCT (Clear Frozen Section Compound, VWR) at 4°C. Samples were then embedded in 1:1 20% sucrose:OCT by flash freezing on dry ice (and kept at -20 until sectioning). Cryosection blocks were cut at a thickness of (6 μm) utilizing the CryoStar NX70 Cryostat by Thermo Fisher Scientific. Slides were stored at -20°C.

2.6 RNA extraction from calvaria

Calvaria were collected and carefully dissected. Dissected calvaria were stored at -20°C in RNA later until they were used to extract RNA. Half of the calvaria was placed into 500μL of TRIzol and homogenized for 45 seconds in a 2mL tube while swirling the sample to mix. Between samples of different genotypes, the homogenizer was rinsed with DEPC treated water and TRIzol (Thermo Scientific). After homogenization, the samples were transferred to new tubes, avoiding any large particles settled at the bottom. RNA extraction was performed according to the manufacturer's instructions.

Resulting RNA pellets were re-suspended in 10μL 0.1% diethylpyrocarbonate (DEPC) water and the concentration was quantified using a NanoDrop 1000 Spectrophotometer (Thermo Fisher Scientific).

2.7 Protein extraction from the organic Trizol phase

Proteins were extracted from the Trizol phase after the RNA extraction protocol. First, the aqueous phase was removed, and ethanol 100% was added to precipitate out unwanted DNA and debris. Samples were incubated for 2-3 minutes at room temperature then centrifuged at 2,000rpm for 5 minutes at 4℃. The phenol-ethanol supernatant was isolated. Isopropanol was added to precipitate proteins. and incubated for 10 minutes at room temperature (RT). The protein pellet was washed three times with 0.3M guanidine hydrochloride for 20 minutes and centrifuged at 3,000rpm for 5 minutes at 4℃. After three wash cycles, the pellet was washed with ethanol 100% and then re-suspended in the cell lysis buffer NP-40 (nonyl phenoxypolyethoxylethanol) cell lysis buffer (50 mM Tris-HCl (pH 7.4), 150 mM NaCl, 1 mM EDTA, 1% (v/v) NP-40) with 1% protease cocktail inhibitor (Sigma). Samples were sonicated and crushed using manual homogenizers. Finally, proteins were combined with 4X Laemmli buffer (200 mM Tris-HCl pH 6.8, 8% SDS, 40% glycerol, 50mM EDTA, 0.08% bromophenol blue) with 5% β- mercaptoethanol, boiled for 10 minutes, spun down and stored at -20℃.

2.8 Serum collection and biochemical analysis

Blood samples were collected by cardiac puncture under deep isoflurane anesthesia. Tubes with whole blood were spun down at 7,000 rpm for 15 minutes at 4℃. The supernatant (serum) was frozen at -80℃. Serum was transported on dry ice to be analyzed for a panel of different bone and metabolic makers at the Comparative Medicine and Animal Resources Centre

(CMARC) at McGill University. A total biochemistry panel was run which includes Albumin, AST, BUN, Phosphorus, Creatinine, Na, K, CI, magnesium, protein, alkaline phosphatase, ALT, bilirubin, calcium, CK, glucose and cholesterol.

2.9 Immunohistochemistry on paraffin-embedded sections

For immunohistochemistry of paraffin 12-week-old femur sections, slides were de-paraffinized with xylene incubations of 3 x 3 minutes. Slides were rehydrated with decreasing ethanol concentration incubations, of 5 minutes each, as follows: 100% ethanol, 95% ethanol, 70% ethanol, 50% ethanol, 30% ethanol and dH_2O. Sections were washed with 1x PBS and then endogenous peroxidases were blocked using Dako Dual Endogenous Enzyme Block. Sections were blocked for 1 hour in 5% skim milk/PBS and then were incubated in hBRIL primary antibody at a 1/4000 dilution in 1% skim milk/PBS. Sections were treated with Envision + System – HRP Labelled Polymer Anti-Rabbit secondary antibody (Dako) for 1 hour and then developed utilizing the Liquid DAB + Substrate Chromogen System (Dako), as per the manufacturer's instructions. Sections were counterstained with hematoxylin dried and mounted with Microkitt (Mecalab Ltd). All incubations were performed at room temperature and all slides were imaged on a Leica DMRB microscope equipped with an Olympus DP70 digital camera. Images of the slides were taken at 2.5x magnification to obtain a broad overview of the femur. Magnified images taken at 40x and then 100x were used to visualize the localization of the resulting signal in more detail. The magnified images presented were taken in the cortical region of the femur. The pattern as well as the intensity of the staining were observed.

2.10 Real time quantitative PCR (RT-qPCR)

Complementary DNA (cDNA) was prepared from the extracted RNA samples using the High Capacity cDNA Reverse Transcription Kit (Applied Biosystems). Reactions were prepared in 20µl using 2µg of RNA according to the manufacturer's protocol. The PCR conditions were set as follows: 25°C for 10 minutes, 37°C for 120 minutes and 85°C for 5 minutes. The resulting cDNA was diluted 1:5 in Milli-Q water (Millipore). Real-time PCR reactions of 20µl were prepared in duplicates in MicroAmp Optical 96-well Reaction Plates (Applied Biosystems) using TaqMan Fast Advanced Master Mix and TaqMan Probes (Applied Biosystems). Plates were run and analysed on a 7500 Real Time (Applied Biosystems) or a QuantStudio 7 flex (Applied Biosystems) PCR System using the Relative Quantification (ddCt) assay. The TaqMan probe for mouse β-actin (Actb) was used as endogenous gene control. The list of probes used in the context of this project is in Table 3.

Table 3: List of TaqMan probes

Gene symbol	Gene name	TaqMan ID
Actb	Mouse β-actin	4352933-0808024
Adipoq	Mouse Adiponectin	Mm00456425_m1
Alpl	Mouse Alkaline phosphatase liver/bone/kidney	Mm00475834_m1
Atf6	Mouse activating transcription factor 6	Mm01295319_m1
Bglap	Mouse osteocalcin	Mm03413826_mH
Bril	Mouse bone-restricted Ifitm-like	Mm00804741_g1
BRIL	Human bone-restricted Ifitm-like	Hs00416846_m1
Col1a1	Mouse Collagen type I, alpha I	Mm00801666_g1
Creb3l1	CAMP Responsive Element Binding Protein 3 Like 1	Mm00496405_m1
Fabp4	Mouse fatty acid binding protein 4	Mm00445878_m1
Ibsp	Mouse integrin-binding sialoprotein	Mm00492555_m1

Notum	Mouse Palmitoleoyl-Protein Carboxylesterase	Mm01253273_m1
Ptgs2	Mouse prostaglandin-endoperoxide synthase 2	Mm00478374_m1
Serpinf1	Mouse serpin family F member 1	Mm00441270_m1
Sost	Mouse sclerostin	Mm04208528_m1
TNSRSF11b	TNF receptor superfamily member 11b (OPG)	Mm00435452_m1
Wif1	WNT Inhibitory Factor 1	Mm00442355_m1
Xbp1	Mouse X-box binding protein 1	Mm00457357_m1

2.11 Western blot

Protein samples were heated and then loaded onto home-made 1mm thick SDS-polyacrylamide gel and migrated by electrophoresis (PAGE) (concentration dependant on the protein of interest) in Tris-glycine SDS running buffer. Proteins were transferred to 0.45µm nitrocellulose membranes (BioRad Laboratories) for 1 hour at 4 degrees post-migration (100V). Membranes were stained with Ponceau S. Then, membranes were then blocked for 1 hour in PBS with 5% skim milk and 0.05% Tween. Membranes were then incubated overnight with the corresponding primary antibody at 4°C on a shaker. Membranes were washed 3-times for 10 minutes each with PBS-Tween 0.05% and incubated with the secondary HRP-coupled antibody for 1 hour at RT. Detection was carried out using EC Western Blotting Detection Reagent for 5 minutes in the dark. Both primary and secondary antibodies were diluted in PBS with 5% skim milk and 0.05% Tween. In this thesis the following antibodies were used for western blot analysis. All three of these are polyclonal antibodies.

Table 4: Antibodies used for western blot

Antibody type	Antibody	Species	Dilution	Brand
Primary	Anti-mouse BRIL N- term	Rabbit	1/2000	Custom made anti-peptide (MDTSYPREDPRAPSSRK-C)
Primary	Anti-human BRIL N-term	Rabbit	1/4000	Custom made anti-peptide (MDTAYPREDTRAPTPS-C)
Secondary	Anti-Rabbit HRP	Donkey	1/30000	GE Healthcare Cat# NA934V

2.12 Analysis of trabecular bone by ex-vivo μCT

μCT imaging to characterize trabecular bone parameters was performed as previously described in the field[56]. The femur of 8-week-old control or mutant mice was scanned ex vivo with the soft tissue removed. Scans were conducted using a 4.5μm pixel size in a SkyScan 1272 high-resolution μCT scanner located at the Shriners Hospital for Children. Specimens were wrapped in gauze with 70% ethanol for moisture and scanned in line with the vertical axis of the scanner. The x-ray tube potential of the scanner was 58 kV, exposure time was 1375 ms, angular rotation was 0.4° and a 0.25 mm aluminum filter was utilized. Prior to scanning, the length of each femur was measured from the top of the medial condyle to the bottom of the major trochanter utilizing the preview x-ray image. After scanning, raw femur images were reconstructed using the Skyscan NRecon program. Representative coronal images are shown.

2.13 Primary calvarial osteoblast cultures

Breedings were set up to generate pups that would all be Tg^{+};tTA^{+}. Transgene expression was repressed by keeping them on Dox treatment until collection. Calvaria were dissected from

4-5 day old mice, minced and placed together in a dish with 1X PBS. After 2 PBS washes, samples were digested with sterile collagenase P (Roche) at 1 mg/ml in αMEM with antibiotics (penicillin/streptomycin) and antimycotic. Cells released from the first digest were discarded. Calvaria were then digested 5 times (15 min each with rotation in 37-degree incubator). Cells were pooled and kept on ice. Cells were spun down for 5 min at 300 g and resuspended with complete media (aMEM supplemented with 10% FBS and 1× pen/strep (Life Technologies). This media was changed at the end of the day to remove any detached cells or debris. After cell digestion, primary cells were placed in a T75 flask (75 cm^2 surface area) to grow until about 90% confluence. They were trypsinized and re-plated in 6 well plates at a density of 300- 400 thousand cells/ well. Day 0 (D0) was considered the day at which the cells reached confluency and media was changed to the described differentiation media. Cells were collected from D0 until D21 for RNA and protein extraction as well as alizarin red staining. Primary osteoblast cells were differentiated in alpha-MEM media containing 10% FBS, 50ug/mL of ascorbic acid and 3 mM of beta-glycerophosphate. A penicillin-streptomycin (PenStrep) mix was also added at a concentration of 100units/mL Penicillin G Sodium and 100ug/mL Streptomycin Sulfate (Life Technologies). The media was changed every 2-3 days.

2.13.1 RNA extraction from primary OB cells

First, cells were washed three times with PBS. Afterwards, 1mL of Trizol was added to the cell layer. The cell lysates were transferred into Eppendorf tubes. Cell lysates were homogenized by vortexing for approximately 1 minute. Chloroform was added to the homogenates, vortexed again for 1 minute and incubated at room temperature for 2-3 minutes. The samples were then centrifuged for 15 minutes at 13,200rpm at 4°C. The aqueous phase was

recovered, and RNA was precipitated with isopropanol then centrifuged at 13,200rpm for 10 minutes at 4°C. RNA pellets were washed using ethanol 70%, dried for 5-10 minutes and resuspended in 10uL of (DEPC)-treated water. The concentration once again was measured using the NanoDrop 1000 Spectrophotometer (Thermo Fisher Scientific) and stored at -20°C. This RNA was then reverse transcribed, and the resulting cDNA was used in RT-qPCR analysis as mentioned in section 2.10 above. Gene expression was measured over time from D0 to D21. The number of replicate cultures was 3 to 4, depending on the genotype.

2.13.2 Protein collection from primary OB cells

Cells were washed three times with 1X PBS. Proteins were extracted from cultured cell layers using the following cell lysis buffer: 50mM Tris-HCl (pH 7.4), 150mM NaCl, 1mM EDTA, 1% (v/v) NP-40 (nonylphenoxypolyethoxyl-ethanol) with 1% of protease inhibitor cocktail (Sigma Aldrich). Cell layers were homogenized by collecting with a cell scraper, transferred to a microtube, incubated on ice for 10 minutes and vortexed at 5-minute intervals. Homogenates were centrifuged at 13,200rpm for 10 minutes at 4℃. Soluble proteins from the homogenate supernatant were collected and combined with 4x Laemmli buffer (200 mM Tris-HCl pH 6.8, 8% SDS, 40% glycerol, 50mM EDTA, 0.08% bromophenol blue) with 5% β-mercaptoethanol, boiled for 5 minutes and stored at - 20℃.

2.13.3 Alizarin red staining of primary OB cells

Cells were washed three times with 1X PBS. PBS was removed and cold 70% ethanol was gently placed on the cells. The plate was placed at 4℃ for 1hr. Ethanol was rinsed off with water. Alizarin red stain was placed on the cells for 1 min at RT. Alizarin red stain was rinsed off

with water. Excess water was tapped off and air-dried. Images wells were taken with a desktop scanner (Canon). The alizarin red staining was used to obtain a qualitative assessment of mineralization at D14 and D21 and to compare between different cultures. The number of replicate cultures was 3 to 4, depending on the genotype.

2.14 Statistical analysis

Data is expressed as the mean values and standard deviations (SD) as the error bar. Each experiment included multiple samples, each designated by a point on the graph. For gene expression analysis using TaqMan probes, 2-3 replicates were used to calculate the average Ct value. Significance was assessed utilizing an unpaired t-test, as indicated, with a p-value ≤ 0.05 being considered statistically significant. Statistical analyses were performed utilizing GraphPad Prism 9 (GraphPad Software).

CHAPTER 3: RESULTS

3.1 Generation of conditional transgenic mouse models expressing hS40L-BRIL or hMALEP-BRIL

The purpose of my studies is to gain knowledge on the *in vivo* role of *BRIL* and to delineate the mechanism by which MALEP-BRIL and S40L-BRIL lead to type V and atypical type VI OI respectively. To do this, we successfully generated transgenic mouse models expressing the human S40L-BRIL (hS40L-BRIL) and the human MALEP-BRIL (hMALEP-BRIL). As an additional control, another model was generated that expressed the wild-type human BRIL (hWT-BRIL). In these models, the transgene is activated when mice are put on a regular diet (on), or repressed (off) by administration of doxycycline (Dox)-containing food/water. This is a Tet-Off system (Figure 4).

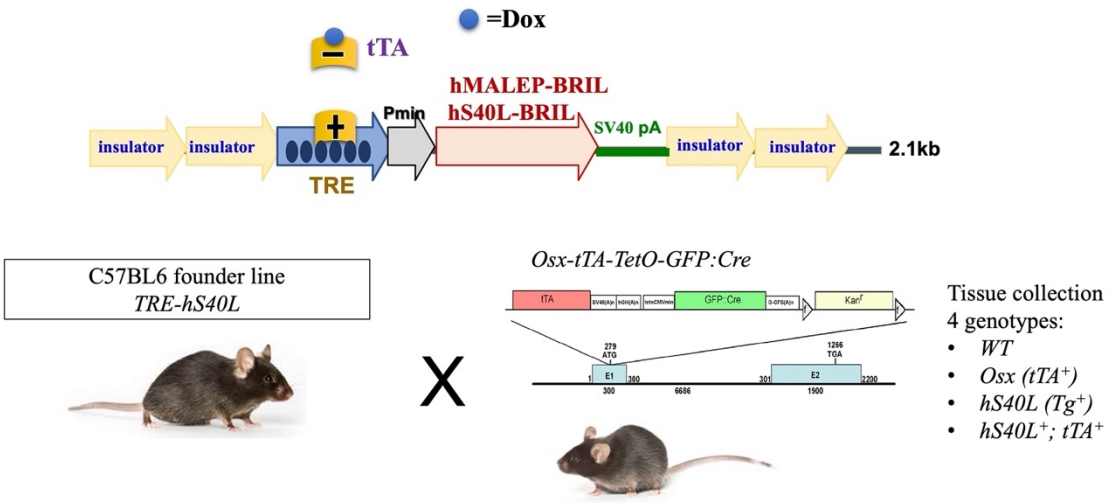

Figure 4: Transgenic construct used to generate the conditional mouse models.
The transgenic construct is presented in schematic form at the top, showing the various elements. These transgenic mice (here the hS40L as an example) are then crossed with the Osx-tTA-Cre mouse model, which contains the tTA under the regulation of the osterix promoter, being expressed in mesenchymal osteoprogenitors at around E13.0. This produces the indicated

genotypes where the Tg^+;tTA^+ are the animals that will express the given transgene in cells where the Osx-Cre is expressed (if Dox is not present). All other animals, not expressing any of BRIL transgenes, are collectively used as controls.

The transgene contains the tetracycline response element (TRE) fused to a minimal CMV promoter, together driving the expression of the transgene (either *hS40L-BRIL, hMALEP-BRIL* or *hWT-BRIL* cDNA). As an additional feature allowing spatial control of expression, the transgenic mice must be crossed with another mouse line containing the tetracycline-controlled trans activator (Osx-tTA-GFP:Cre). When doxycycline (Dox) is present, it binds to the tTA, removing it from the TRE and inhibiting the expression of the transgene. We chose to cross these transgenic models with the Osx-Cre mouse model, which contains the tTA in the transgene and is expressed mostly in osteoblasts (and in some growth plate hypertrophic chondrocytes)[53]. It also contains GFP, therefore we were able to visualize the tTA^+ (Osx-Cre) cells and therefore the transgene using fluorescence microscopy.

3.2 Expressing *hS40L-BRIL* or *hMALEP-BRIL* from conception in embryos

3.2.1 Skeletal staining of late-stage E18.5 embryos and histological assessment

Transgenic mice expressing either the human S40L-BRIL, MALEP-BRIL, or WT-BRIL were produced using the same transgenic construct (shown in Figure 3) and technique (section 2.1). For each transgene, 3 independent lines were analyzed to exclude to possibility of transgene expression levels, or confounding effects of the integration sites. Each of these was crossed with Osx-Cre (tTA^+) mice and the mothers were not exposed to Dox. Embryos (E18.5) were collected for gene expression analysis via qPCR, histology, and skeletal staining. Overall, at least 2-3 complete litters were collected for each model at E18.5. N=3-4 embryos expressing the transgene

(either hS40L-BRIL or hMALEP-BRIL) and multiple controls (N=4-6 per litter) were analyzed in this report. Data from replicate experiments with the same model were consistent.

Skeletons were stained with alizarin red/alcian blue once soft tissue was cleared. Images of the whole-body skeletal staining were taken on a benchtop microscope (Leica MZ6) and representative images from these skeletal preparations for each model are presented in Figure 5.

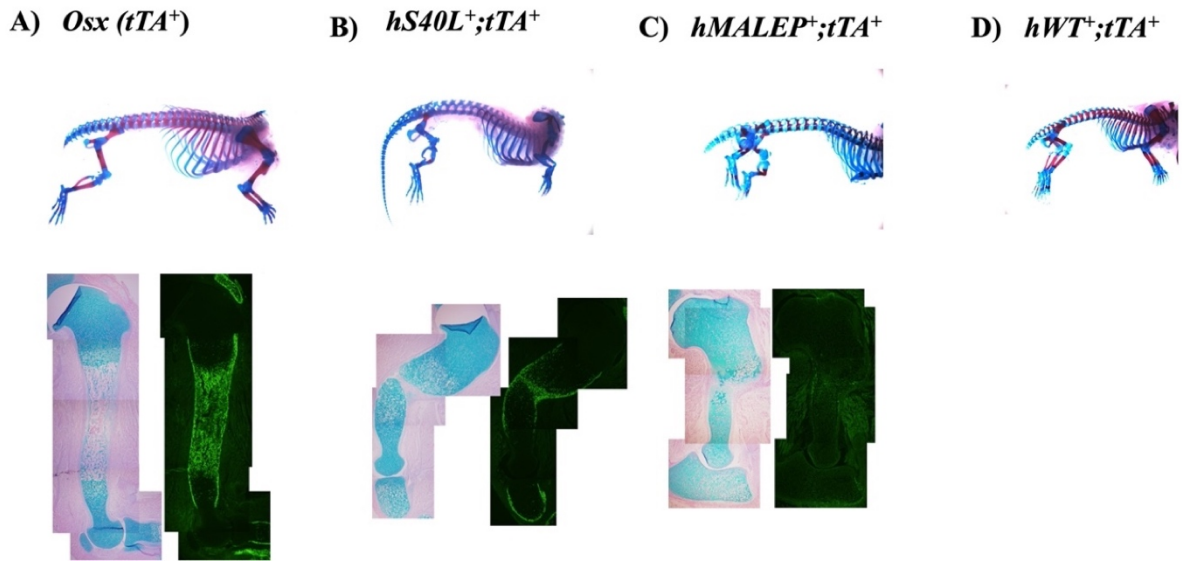

Figure 5: Expression of either hS40L-BRIL, hMALEP-BRIL, or hWT-BRIL from conception results in skeletal deformities and neonatal lethality.
The top panels show the whole skeleton alizarin red/alcian blue staining of E18.5 embryos. Bent long bones of the fore- and hind-limbs are visible only in the hS40L and hMALEP. One representative line shown for each transgene. Bottom panels show the histological architecture of the humeri from each of the genotype (except hWT-BRIL), showing alcian blue staining with the corresponding GFP fluorescence signal coming from the Osx-tTA-Cre.

Expressing either hS40L-BRIL or hMALEP-BRIL from conception led to an overall decrease in mineralized bone. There is a decrease and restriction in the region stained with alizarin red. As shown in Figure 4 B) and C) the long bones are also hypo mineralized with little alizarin red staining and are bent. Expressing hS40L-BRIL or hMALEP-BRIL from conception was consistently neonatal lethal, likely because of an extremely hypo-mineralized rib cage. This

lethality was predicted based on observations in previous models for OI type V[48,49]. The mice expressing the hWT-BRIL, however, did not show any visual skeletal abnormalities and were not different from the control embryos. The forelimbs of the hS40L-BRIL and hMALEP-BRIL E18.5 embryos were sectioned using a cryostat. Sections were stained using a 0.1% alcian blue in 0.1M HCl solution. GFP fluorescence was visualized by fluorescence microscopy. A representative image is shown of a full slide from each genotype in Figure 4 (A), (B), and (C). Histological assessment of the E18.5 humeri expressing either *hS40L-BRIL* and *hMALEP-BRIL* show that they were filled with hypertrophic chondrocytes and presented with Osx:GFP^{+} cells at a wedge-like pattern in the mid-shaft region (Figure 4 B/C). This agreed with what was also observed in the previous OI type V knock in model from our laboratory[49].

3.2.2 Gene expression analysis on E18.5 embryonic calvaria

RT-qPCR analysis of E18.5 hS40L-BRIL and hMALEP-BRIL calvaria was performed using TaqMan probes for key osteoblast genes, such as *Bglap*, *Ibsp* and *mBRIL*. Western blots were also performed. Gene expression analysis for the E18.5 hS40L-BRIL and hMALEP-BRIL embryos is shown in Figure 6. Gene expression analysis for the hS40L-BRIL (Figure 6A) and the hMALEP-BRIL (Figure 6B) show significantly decreased expression of osteoblast differentiation markers *Bglap*, *Ibsp* and *mBRIL* in the mutants relative to the controls. *Ptgs2* is upregulated in both mutant models as compared to the controls. This suggests an overall halt in differentiation and an increased inflammation process. We observed a consistent reduction in the endogenous mouse *Bril* expression and attenuated mBRIL protein levels in the hS40L mutant calvaria, but not so much so in the hMALEP-BRIL. The western blot shown in Figure 6B also indicate the slower mobility of the hMALEP-BRIL due to its 5 amino acid extension. Together,

these data indicate that expressing either hS40L-BRIL or hMALEP-BRIL from conception leads to a decrease in osteoblastogenesis and a distorted skeleton, leading to neonatal lethality.

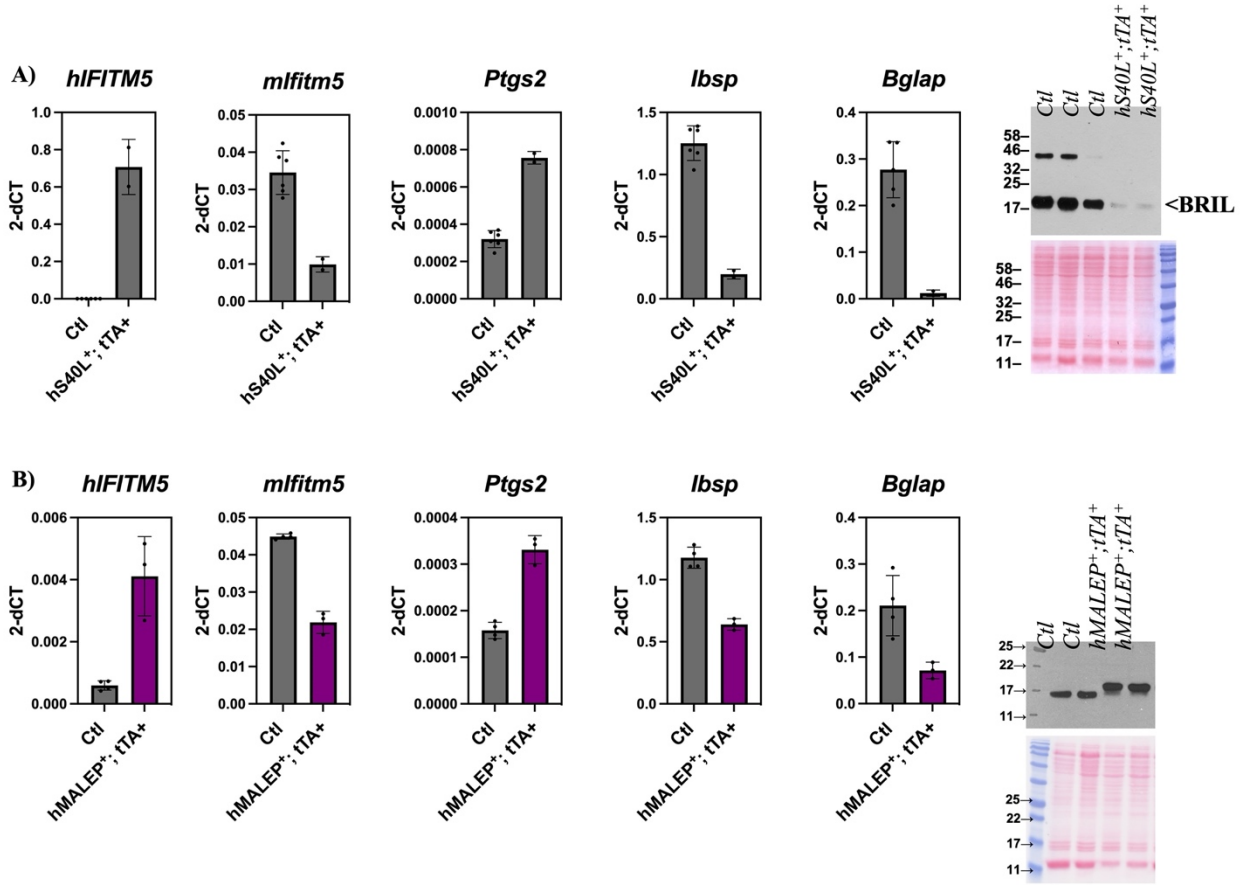

Figure 6: Decreased expression of osteoblastogenesis markers in E18.5 hS40L+;tTA+ and hMALEP+;tTA+ embryos.

Gene expression by RT-qPCR and western blot analyses on calvaria samples from the hS40L-BRIL (A) and hMALEP-BRIL (B) E18.5 embryos. The qPCR data are expressed as $2^{-\Delta Ct}$ normalized to β-actin levels (n=3-4). Western blots on calvaria protein samples using an anti-BRIL primary antibody are shown at right, for 2 controls and 2 mutants.

3.3 Osteoblast cultures

To further investigate the cell-autonomous effects of hS40L-BRIL and hMALEP-BRIL, newborn calvarial osteoblast cultures from each mouse model were established. For this purpose, because of the neonatal lethality, mothers with pups were kept on Dox to repress expression of the transgenes until collection on day 4-5. At time of seeding, the cells were grown in the absence of Dox, allowing the transgene of interest to be expressed. Differentiation media was placed on the cells as of seeding into 6-well plates. Samples were collected from D0 (confluency) to D21 of differentiation to assess mineralization by alizarin red staining, extract RNA, and extract cellular proteins for western blotting.

3.3.1 Alizarin red staining of osteoblast cultures

Alizarin red staining was performed at D14 and D21 to obtain a qualitative assessment of mineralization. Representative images for one culture are shown in Figure 7A. There was significantly less alizarin red staining at D14 and D21 in the hMALEP-BRIL cultures, while the hS40L-BRIL cultures presented with little to no staining. In contrast, the hWT-BRIL primary culture mineralized more than the hS40L-BRIL or the hMALEP-BRIL, but not to the same extent as the control culture. Western blotting performed on the cell layers (Figure 7B) indicated that there were about equal levels of the various human BRIL proteins being produced in each culture. The antibody used here was selective for the human BRIL protein, and consequently poorly detected the endogenous mouse BRIL in the control cells.

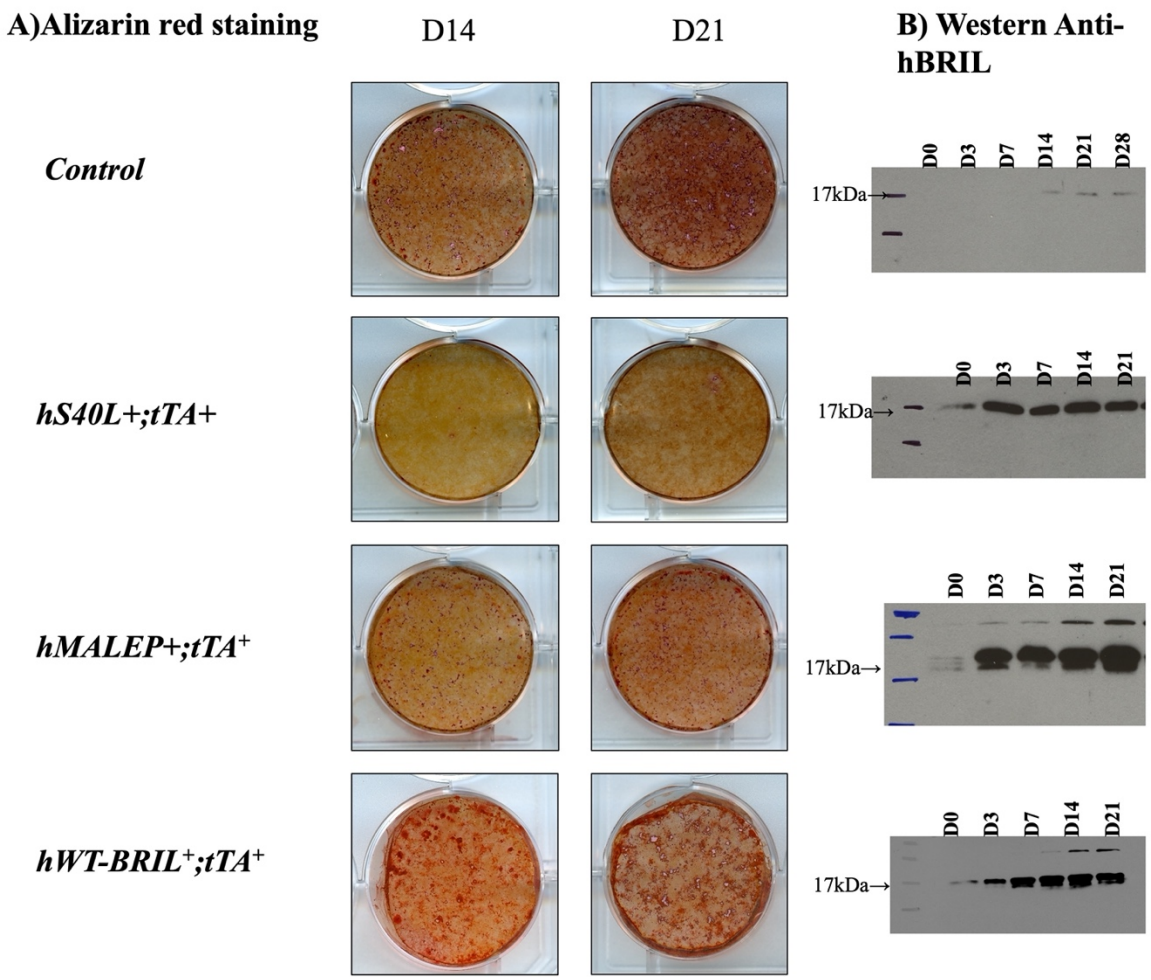

Figure 7: Alizarin red staining and BRIL protein expression in osteoblast cultures from the different models.

Alizarin red staining (A) was performed on all the osteoblast cultures collected from the various models. The panels are from one representative experiment performed on triplicate cultures. Representative western blot detection (B) of the human BRIL proteins from the cell layers for each culture.

3.3.2 Gene expression analysis in the osteoblast cultures

Gene expression analysis using RT-qPCR was performed for each of the primary osteoblast cultures, except the hWT-BRIL. Figure 8 presents the relative expression levels over the time-course (days 0, 3, 7, 14 and 21) of the cultures for *hBRIL* (transgenes) as well as osteoblast markers (*mBril, Alpl, Ibsp* and *Bglap).* The expression levels of hMALEP-BRIL and hS40L-BRIL did not

differ significantly across all time points (Figure 8A). For *mBril*, *Alpl*, *Ibsp*, and *Bglap* (Figure 8B to D), both the hMALEP and hS40L cultures had significantly decreased expression as compared to control cultures. In the hS40L, however, the levels were consistently lower than in the hMALEP. Overall, these results indicate that the effect of both mutant BRIL is cell autonomous.

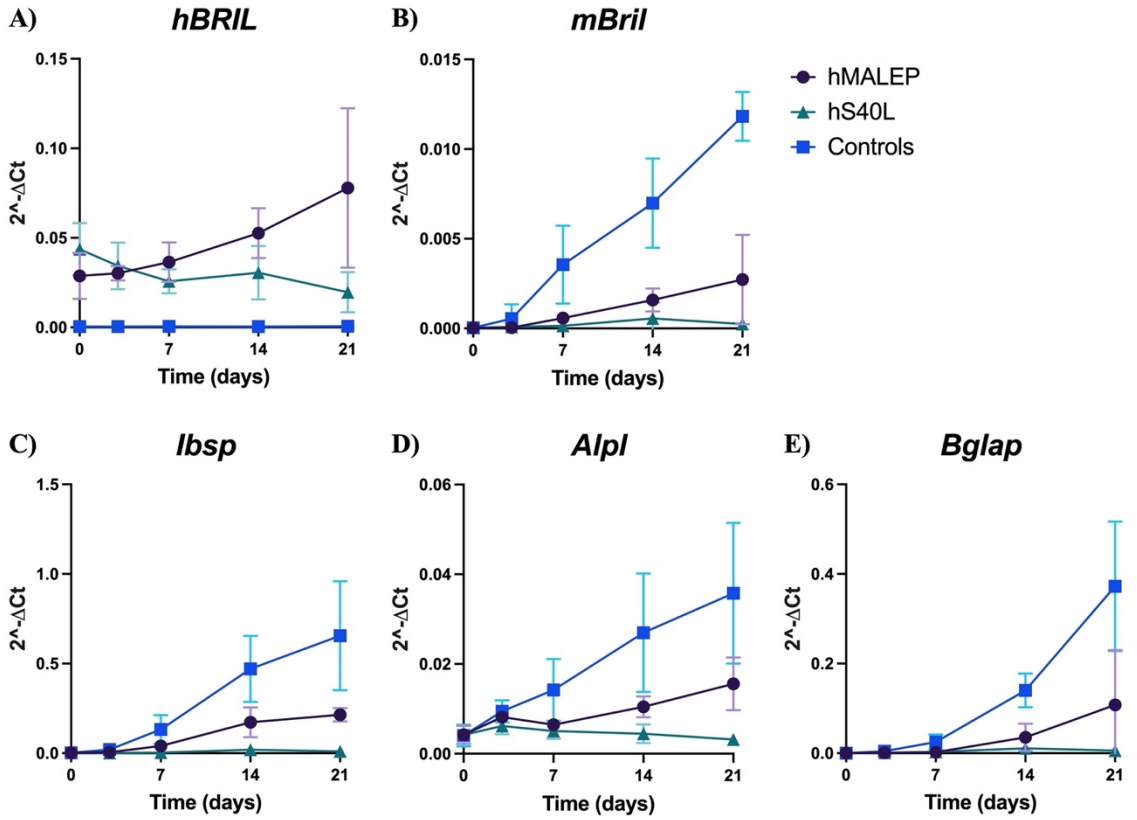

Figure 8: Expression of osteoblast differentiation markers in osteoblast cultures. Cultures from the hMALEP, hS40L and controls were collected at day 0, 3, 7, 14, and 21. The RNA was extracted and RT-qPCR performed to monitor expression of human *BRIL* transgenes, and endogenous mouse *Bril*, *Ibsp*, *Alpl*, and *Bglap*. The graphs show the relative expression at each time point ($2^{-\Delta Ct}$ normalized to *b-actin*). Each point represents the mean value and the error bars represent the SD between replicate cultures in that group (n=3 to 4).

3.3.3 Expression of *Col1a1*, *Serpinf1* and adipogenic markers *Adipoq* and *Fabp4* in hS40L-BRIL cultures

Next, gene expression analysis of some additional genes in the hS40L-BRIL cultures was assessed. *Col1a1* was used because of the observed decrease in mineralization visualized in the cultures. *Serpinf1* was assessed due to the hypothesized link between BRIL and PEDF, as described in the introduction. There was a significant decrease, from day 3 to day 21, in the expression levels of *Serpinf1* and *Col1a1* in the hS40L-BRIL osteoblasts compared to controls. Microscopic examination of the hS40L-BRIL osteoblasts indicated the possibility of having an increased number of cells with a morphology resembling adipocytes. Two markers of adipocytes (*Adipoq* and *Fabp4*) were analyzed to determine if this was due to a shift of the cultures toward adipogenesis. As presented in Figure 9C and D, the expression levels of these two markers were increased relative to controls. However, the heterogeneity of the results made the differences not statistically different.

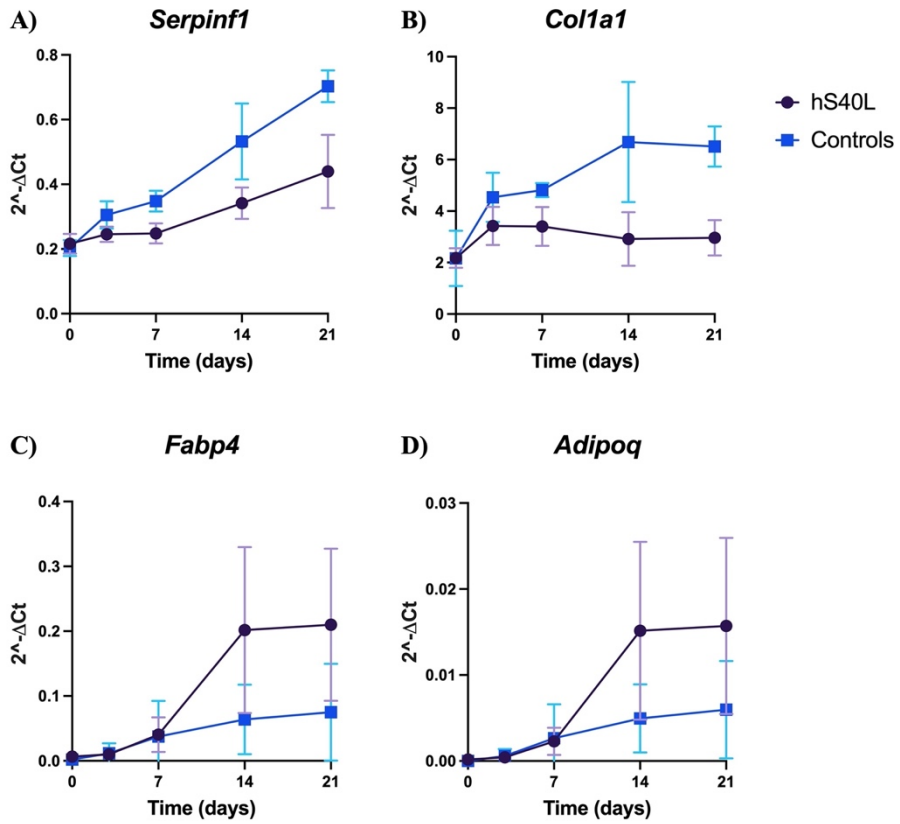

Figure 9: Expression of *Serpinf1*, *Col1a1*, and adipogenic markers *Adipoq* and *Fabp4* in hS40L-BRIL osteoblasts.

Cultures from the hS40L and controls were collected at day 0, 3, 7, 14, and 21. The RNA was extracted and RT-qPCR performed to monitor expression of endogenous mouse *Serpinf1*, *Col1a1*, *Adipoq*, and *Fabp4*. The graphs show the relative expression at each time point ($2^{-\Delta Ct}$ normalized to *b-actin*). Each point represents the mean value and the error bars represent the SD between replicate cultures in that group (n=4).

Immunofluorescence localization data previously showed that the hS40L-BRIL protein is retained intracellularly in the ER-Golgi network[32]. We hypothesized that this could cause ER stress inducing an unfolded protein response (UPR). Therefore, components of the UPR were assayed in the hS40L-BRIL cultures (Figure 10). Gene expression for various markers of the 3 different UPR pathways, regulated by three master transcriptional regulators, were analyzed by RT-qPCR, namely *Xbp1* and *Edem1* (IRE1 pathway), *Atf4* and *Eif2ak3* (PERK pathway), *Atf6*

and *Pdia4* (ATF6 pathway)[57]. No significant upregulation of UPR markers was observed in hS40L-BRIL cultures over time, as compared to controls. However, significant increases in *Xbp1* (p value=0.0061) and *Eif2k3* (p value=0.0015) in hS40L cultures were observed at D0 (when the cells became confluent). There was also a nearly significant increase (p value=0.0622) seen for *Atf4*. This suggested that an initial stress response may have occurred early in culture, but not persisted in later time points.

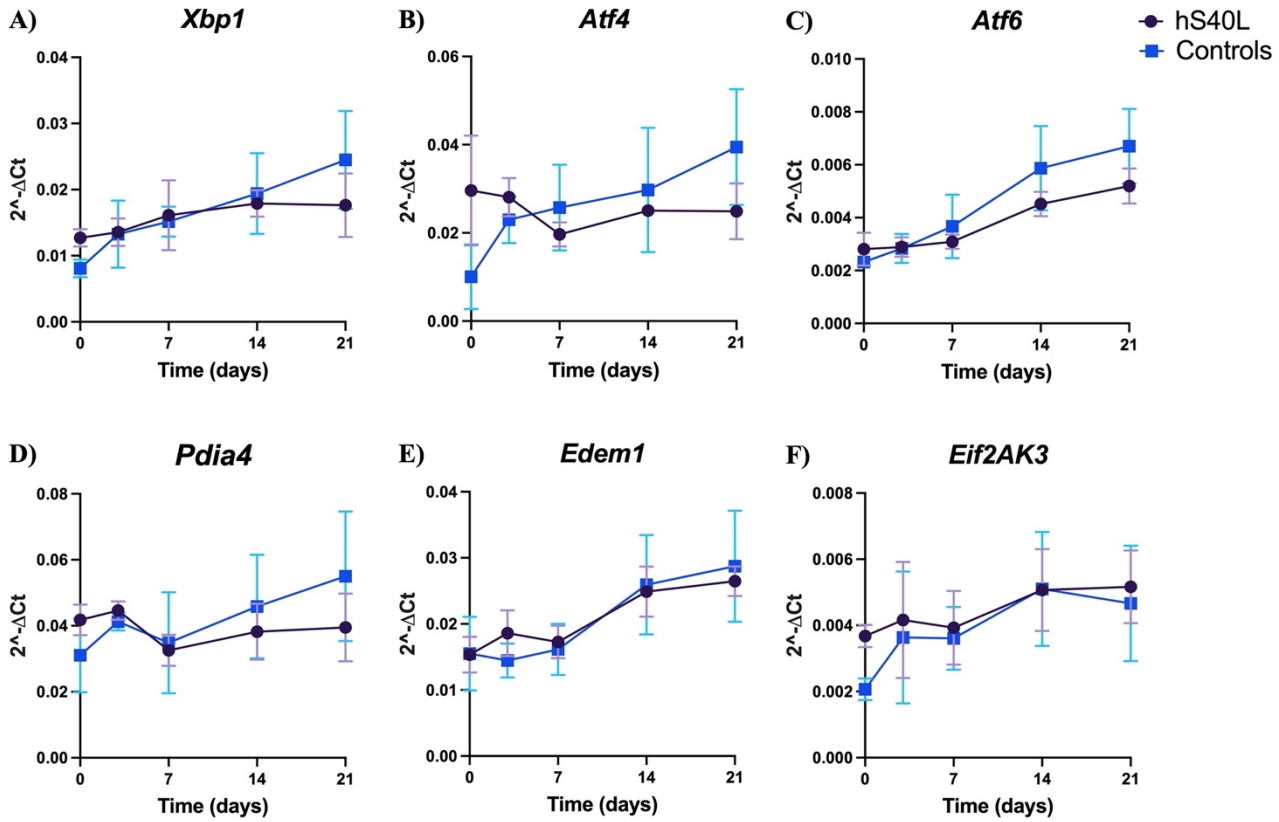

Figure 10: Expression of UPR markers in hS40L-BRIL osteoblasts.
Cultures from the hS40L and controls were collected at day 0, 3, 7, 14, and 21. The RNA was extracted and RT-qPCR performed to monitor relative expression of UPR markers *Xbp1* (A), *Atf4* (B), *Atf6* (C), *Pdja4* (D), *Edem1* (E), and *Eif2ak3* (F). The graphs show the relative

expression at each time point ($2^{-\Delta Ct}$ normalized to *b-actin*). Each point represents the mean value and the error bars represent the SD between replicate cultures in that group (n=4).

3.4 Expressing *hS40L-BRIL* post-natally

The next goal of my work was to characterize the effects of expressing hS40L-BRIL and hMALEP-BRIL post-natally only, due to the peri-natal lethal phenotype when expressed constitutively. First, hS40L-BRIL was expressed from 8-12 weeks, by keeping the mice on Dox in the drinking water until 8 weeks of age. After 4 weeks of expression, the visual appearance of almost all skeletal elements examined (femur, tibia, vertebrae, and mandible) from the hS40L-BRIL model were strikingly bulky and white, as compared to controls. For simplicity only the femurs are presented in Figure 11A. uCT imaging revealed an extensive expansion of the periosteal bone surfaces, with a feathery type of appearance, as well as within the metaphyseal trabecular compartment (Figure 11B). This bulky appearance was found to be partially reversible when mice were put back on Dox for an additional 6 weeks (Figure 11C). In this setting, the uCT imaging revealed significant cortical bone formation through the midshaft, whereby the cortices appeared doubled with some residual trabeculae in between (Figure 11D). Body weight and size of the hS40L-BRIL mice increased towards normal when put back on Dox (data not shown).

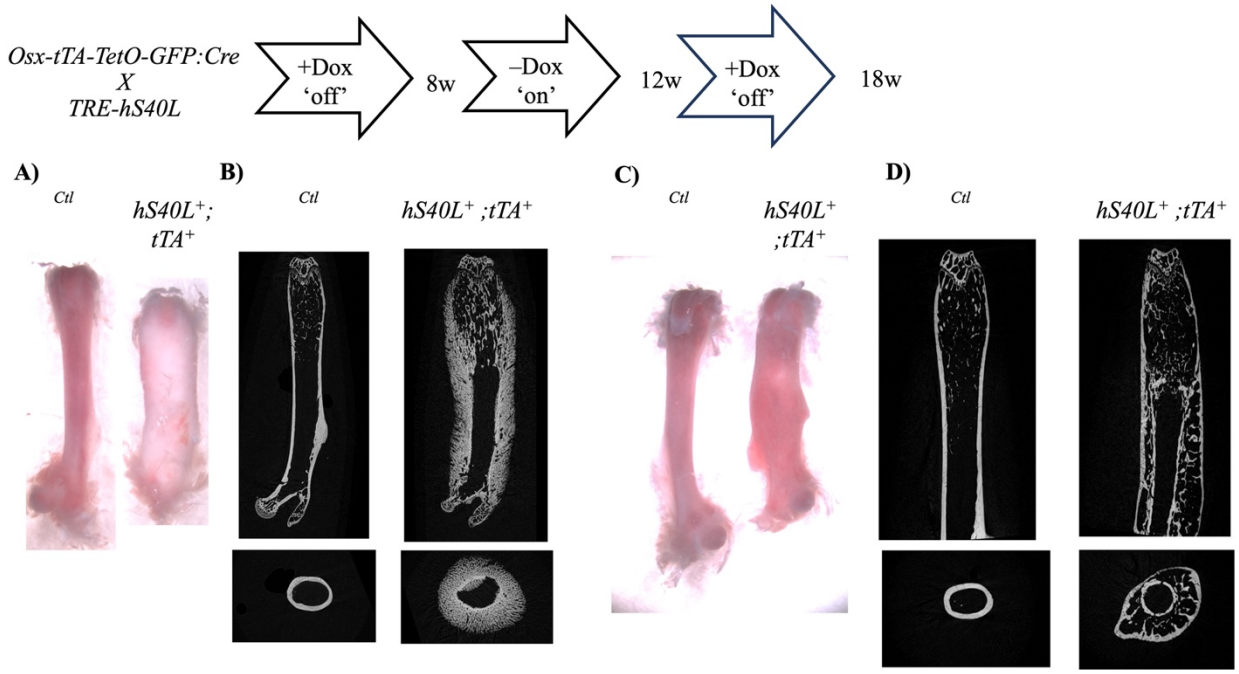

Figure 11: Postnatal expression of hS40L-BRIL causes massive bone accrual that is partially reversible.

A) Dissected femurs from 12-week-old control and hS40L-BRIL mice kept on Dox (repressed) until 8 weeks. B) Representative µCT longitudinal (top) and crossectionnal (bottom) images of femurs from control and hS40L. C) Dissected femurs from 18-week-old control and hS40L-BRIL mice when put back on Dox from 12-18 weeks. D) Representative µCT longitudinal (top) and crossectionnal (bottom) images of femurs from control and hS40L-BRIL.

3.4.1 RNA sequencing of calvaria and tibia from hS40L-BRIL mice off Dox from 8-12 weeks

RNA was isolated from the tibia and calvaria to be purified and sent for RNAseq with the goal of gaining a non-biased broad gene expression perspective. The reads were mapped back to the mouse transcriptome and the genes which were differentially regulated in both the calvaria and the tibia were then grouped together to define pathways of interest[58]. A broad schematic overview of the differentially expressed genes (DEG) and their fold change is presented in Figure 12. A vast list of genes was found differentially expressed between the controls and the hS40L tibia (3723) and calvaria (631), and 580 were common in both tissues (Figure 12A). A

significant fraction of the DEG were increased (214, 3723) or decreased (417, 1423). Among those, a pathway analysis revealed many of the DEG are known regulators of bone formation (*Dmp1*, *Sp7, Alpl, Dlx3, Bmp2, Tnfsf11b*), involved in inhibiting the Wnt pathway (*Notum*, *Apcdd1*, *Wif1*, *Sost*), of related to inflammation and stress (*Ptgs2*, *Creb3l1*) (Figure 12B). All of them excepted sclerostin (*Sost*) were upregulated. The fold changes in the gene expression were next validated by qPCR for some targets (Figure 13). All of them followed the same trends as those detected by bulk RNAseq.

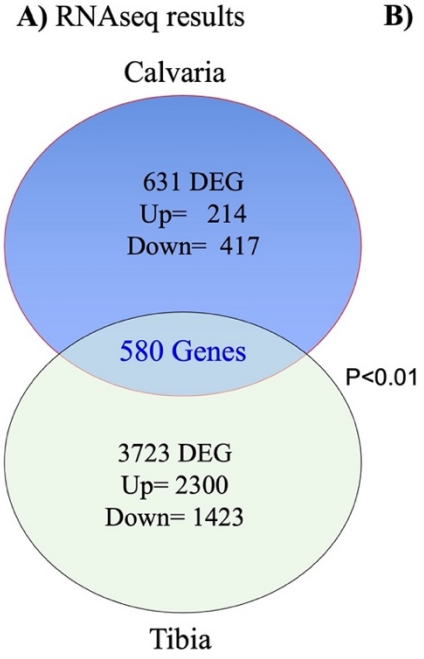

B)

Pathway involved	Gene name	Fold change	p value
Wnt inhibition	*Notum*	26.2	2.3E-32
	Apcdd1	11.7	4.6E-05
	Wif1	6.4	1.5E-12
	Sost	-4.9	3.3E-10
Osteoblast activity	*Dmp1*	10.6	6.5E-07
	Tnfrsf11b (OPG)	8.2	2.2E-06
	Alpl	5.4	5.5E-10
	Sp7 (OSTERIX)	4.3	7.2E-08
	Dlx3	4.2	1.1E-07
	Bmp2	3.5	7.6E-03
	Serpinf1 (PEDF)	3.3	3.3E-05
Inflammation/ stress	*Ptgs2* (COX2)	8.4	2.4E-06
	Creb3l1 (OASIS)	5.3	4.2E-10

Figure 12: RNA sequencing of calvaria and tibia from hS40L-BRIL mice off Dox from 8-12 weeks.

RNA samples from 12-week-old calvaria and tibia of each genotype (controls and hS40L-BRIL) were sent for sequencing and reads were mapped back to the mouse transcriptome (n=3 for each group). A) Schematic representing the number of genes that were differentially regulated in each tissue and the number of genes overlapping which were differentially regulated in both tissues. B) Table of the most relevant bone pathways which were affected. The gene names are included along with fold change compared with the controls and the p-value.

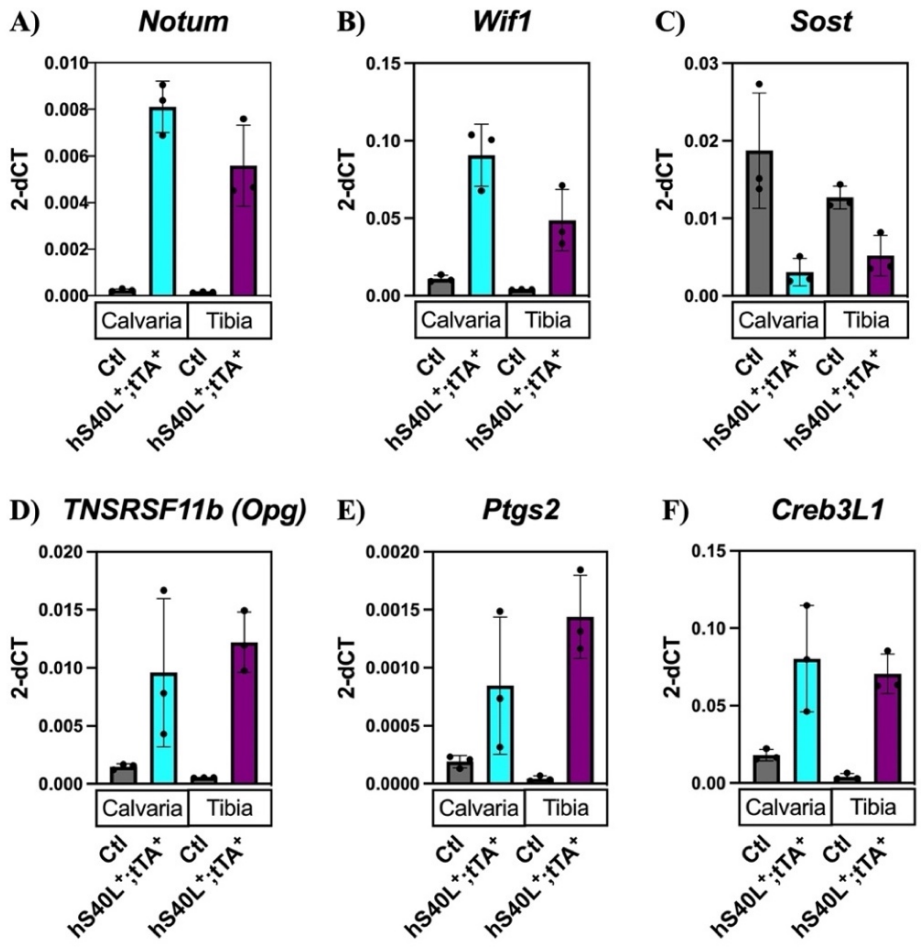

Figure 13: Validation of RNASeq results in calvaria and tibia of mice expressing hS40L from 8-12 weeks.

Gene expression analysis via RT-qPCR with specific TaqMan probes: *Notum* (A), *Wif1* (B), *Sost* (C), *Tnsrsf11b* (D), *Ptgs2* (E), and *Creb3l1* (F). The graphs show the relative expression at each time point ($2^{-\Delta Ct}$ normalized to *b-actin*). Each point represents the mean value and the error bars represent the SD between replicate cultures in that group (n=3).

3.4.2 Comparison of 12-week-old hMALEP-BRIL and hS40L-BRIL mice

Gene expression analysis via RT-qPCR was also performed on tibia samples from 3-month-old mice expressing hMALEP-BRIL. This was to further characterize this bone phenotype as well as to compare to what was seen in the hS40L-BRIL samples shown above.

These data show that there is also a significant increase in expression of *Ptgs2* (13.7 fold increase, p value= 0.0002) and *Tnsrsf11b* (9.2 fold increase, p value= 8.4E-05) as was seen in the previous post-natal hS40L-BRIL samples (Figure 14).

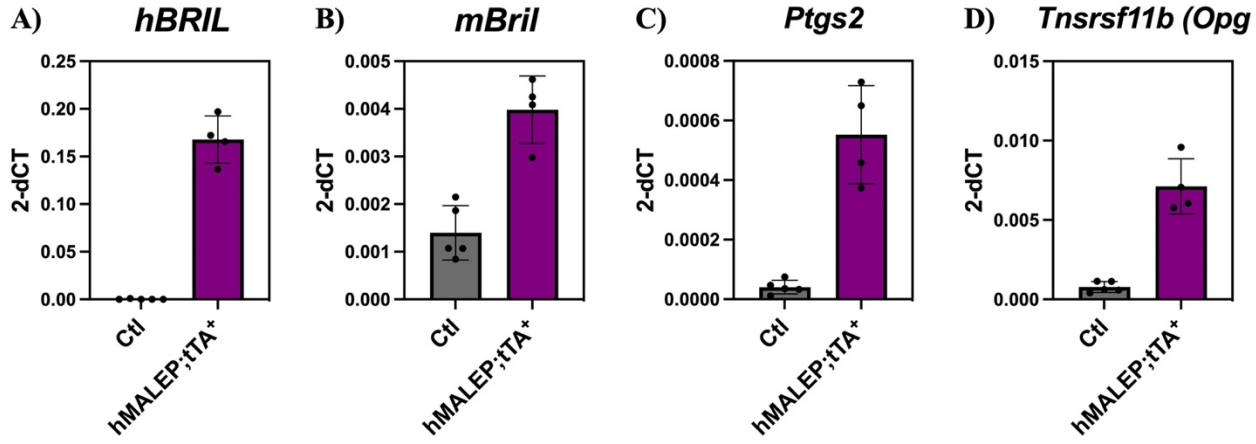

Figure 14: Gene expression in 3-month-old hMALEP-BRIL tibias.
Tibia RNA was reverse transcribed and amplified using gene-specific TaqMan probes by RT-qPCR. β-actin was used as the endogenous reporter gene. Relative expression of *hBRIL* (A), *mBril* (B), *Ptgs2* (C), and *Tnsrsf11b (Opg)* (D).

3.4.3 Serum biochemical analysis on mice expressing *hS40L-BRIL* and *hMALEP-BRIL*

To assess if any gross systemic changes were occurring in either of the mutant models, a full biochemistry panel was run on serum samples of 3-month-old male mice. Most measured indices (albumin, AST, phosphorus, creatinine, sodium, chloride, magnesium, ALT, bilirubin, calcium, creatine kinase, potassium, glucose and cholesterol) were not significantly altered and all values were within normal range (data not shown). The two markers found to be outside of normal range were alkaline phosphatase and blood urea nitrogen (BUN) (Figure 15). The hS40L-BRIL mice had a 5.5-fold increase in serum levels of alkaline phosphatase, while the hMALEP

had a 6.6-fold increase (Figure 14A). Only the hS40L-BRIL showed a significant decrease BUN (2.8-fold decrease relative to an average of 6.2 mmol/L) (Figure 15B).

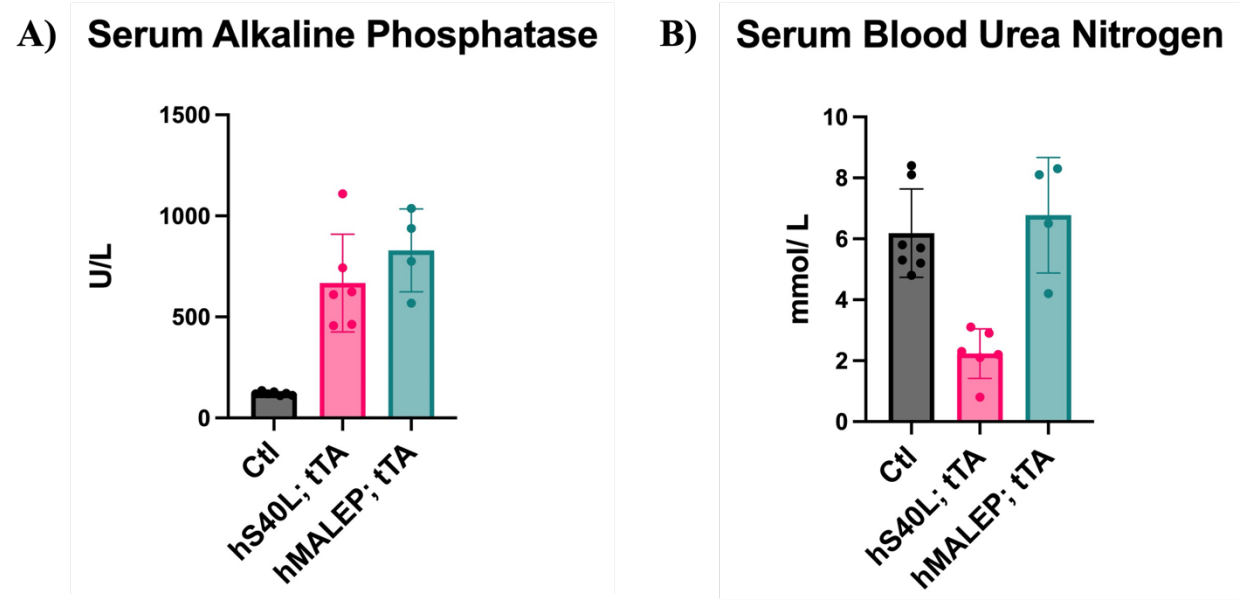

Figure 15: Serum biochemical analysis in mutant mouse serum at 12 weeks.
A) hS40L-BRIL and hMALEP-BRIL samples show increased levels of alkaline phosphatase. B) hS40L-BRIL show a decrease in BUN levels. Each point on the graph represents a sample and the horizontal lines represent the mean value of the samples in that genotype (n=4-6)

3.4.4 Histology and immunohistochemistry of hS40L-BRIL and hMALEP-BRIL

In order to further characterize the post-natal phenotype of the hS40L-BRIL and hMALEP-BRIL mice, a histological and immunohistochemical approach was undertaken. This would allow also to validate whether the distribution pattern of the hS40L-BRIL, reported to be trapped in the ER-Golgi in vitro, could be visualized in vivo. As an additional control, we had in the meantime generated transgenic mice expressing the human wild type form of BRIL (hWT-BRIL) to serve as 'negative' controls. This was done to exclude the possibility that different expression levels of the different transgenes could lead to the exacerbated phenotype described

above, and not be related to the genotypes (hS40L and hMALEP). Femurs from control (tTA), hS40L-BRIL, hMALEP-BRIL and the newly obtained hWT-BRIL were collected from 3-month-old mice that were taken off Dox at birth. Paraffin embedded femurs were sectioned and processed for picrosirius red staining, to visualize the collagen fibers, and for immunohistochemistry to detect the hBRIL proteins (Figure 16). Sirius red staining confirmed that the exuberant periosteal and trabecular material produced in the hS40L-BRIL and hMALEP-BRIL is collagenous (Figure 16 left panels). Immunostaining for the hBRIL protein in the control (non-transgenic) mice (Figure 16 A) gave a weak signal, possibly detecting the endogenous mBRIL protein. The intensity was strong for the hS40L-BRIL and the hMALEP-BRIL (Figure 16 B, C), especially on bone forming surfaces and also in embedded cells. The staining for the hS40L-BRIL looked more punctate (rounded in shape) when compared to the hMALEP. However, subcellular localization of the hS40L-BRIL in the Golgi was not confirmed using these *in vivo* paraffin sections because of the lack of resolution. An interesting but unexpected observation was that the hWT-BRIL femur seemed to also display an expanded collagenous matrix as demonstrated by the increase surface area of the picrosirius stain along the midshaft (Figure 16D). The immunostaining for hBRIL protein in the hWT-BRIL femur was also strong on cells abutting bone surfaces (Figure 16D).

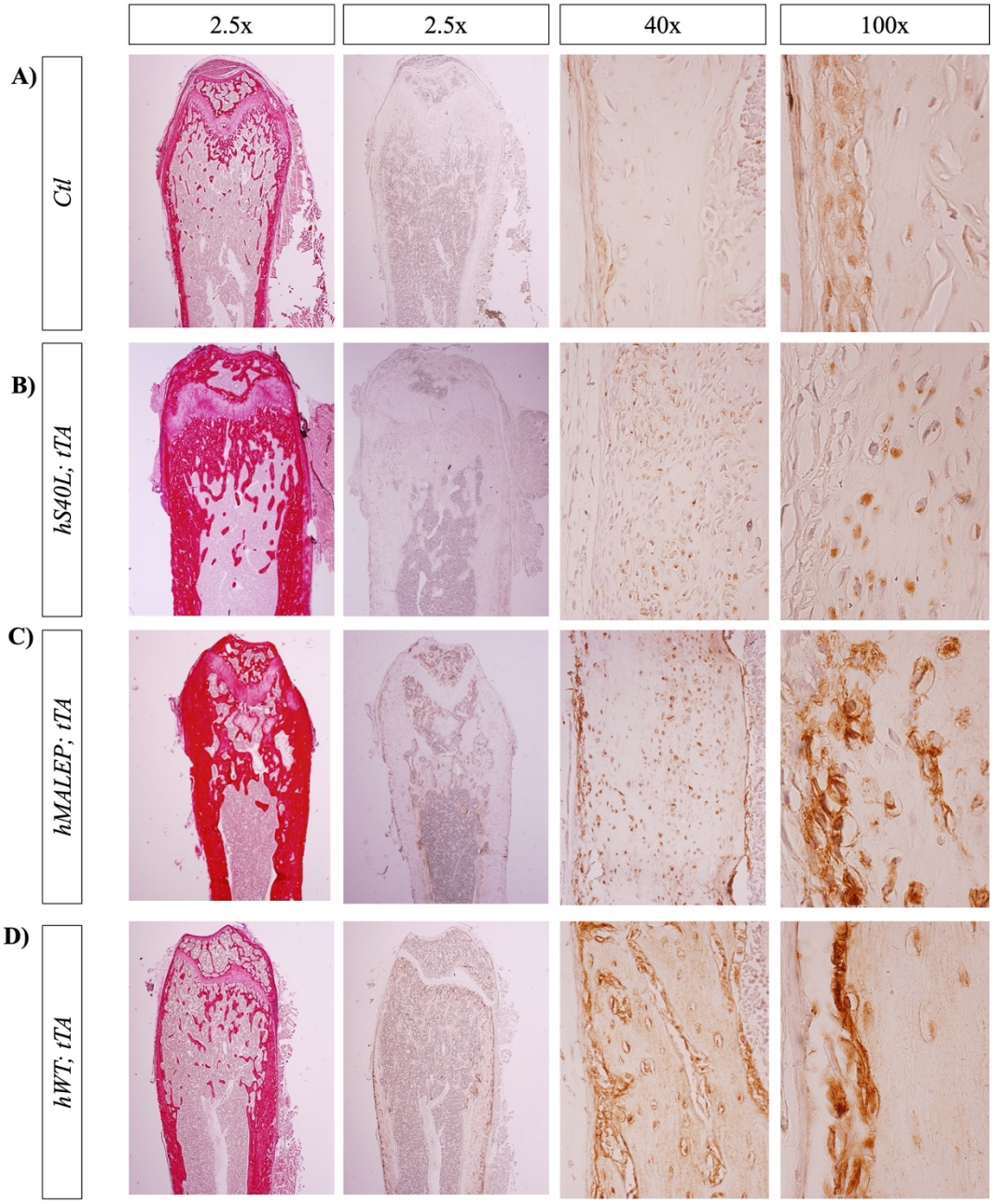

Figure 16: Histological and immunolocalization for hBRIL protein in sections of 3-month-old femurs.

Sirius red staining (left panels) and immunolocalization for hBRIL (right panels) in femurs at 3 moths from controls (A), hS40L (B), hMALEP (C), and hWT (D). The magnification of pictures (2.5, 40, and 100X) for the immunostaining are indicated at the top.

3.4.5 Comparing *hS40L-BRIL*, *hMALEP-BRIL,* and *hWT-BRIL* post-natally at 12 weeks.

To determine whether the phenotypic effects observed for the hS40L-BRIL mice was specific for this genotype, we next compared and analyzed the phenotypes of the hS40L-BRIL to that of hMALEP-BRIL, as well as of the hWT-BRIL because it did present with a phenotype (Figure 15). For this purpose, mice were taken off Dox at birth and collected at 3 months of age. To be thorough, the phenotypic characterization was conducted systematically in 3 independent transgenic lines for each of the 3 genotypes (hS40L-BRIL, hMALEP-BRIL, and hWT-BRIL). Representative images of femurs from these mice are shown in Figure 17. For the 3 hS40L-BRIL lines, the bone appearance was chalky white and accrual was equally massive as compared to controls (Figure 17A). For the 3 hMALEP-BRIL lines, only the lines Q21 and Q151 presented with a similar bone expansion and white coloration (Figure 17B). The third line (Q158) appeared no different from the controls, but it was found not to express the hMALEP-BRIL transgene (data not shown). Unexpectedly, the 3 hWT-BRIL transgenic mouse lines also presented with a similar phenotypic appearance, although it was more variable (Figure 17C). In this model the 866 line did not show any visual bone expansion whereas animals from the 874 line show severe expansion. These results suggested that the postnatal phenotypes of the hS40L-BRIL and hMALEP-BRIL were not related to pathogenic effects as they were indistinguishable from the hWT-BRIL.

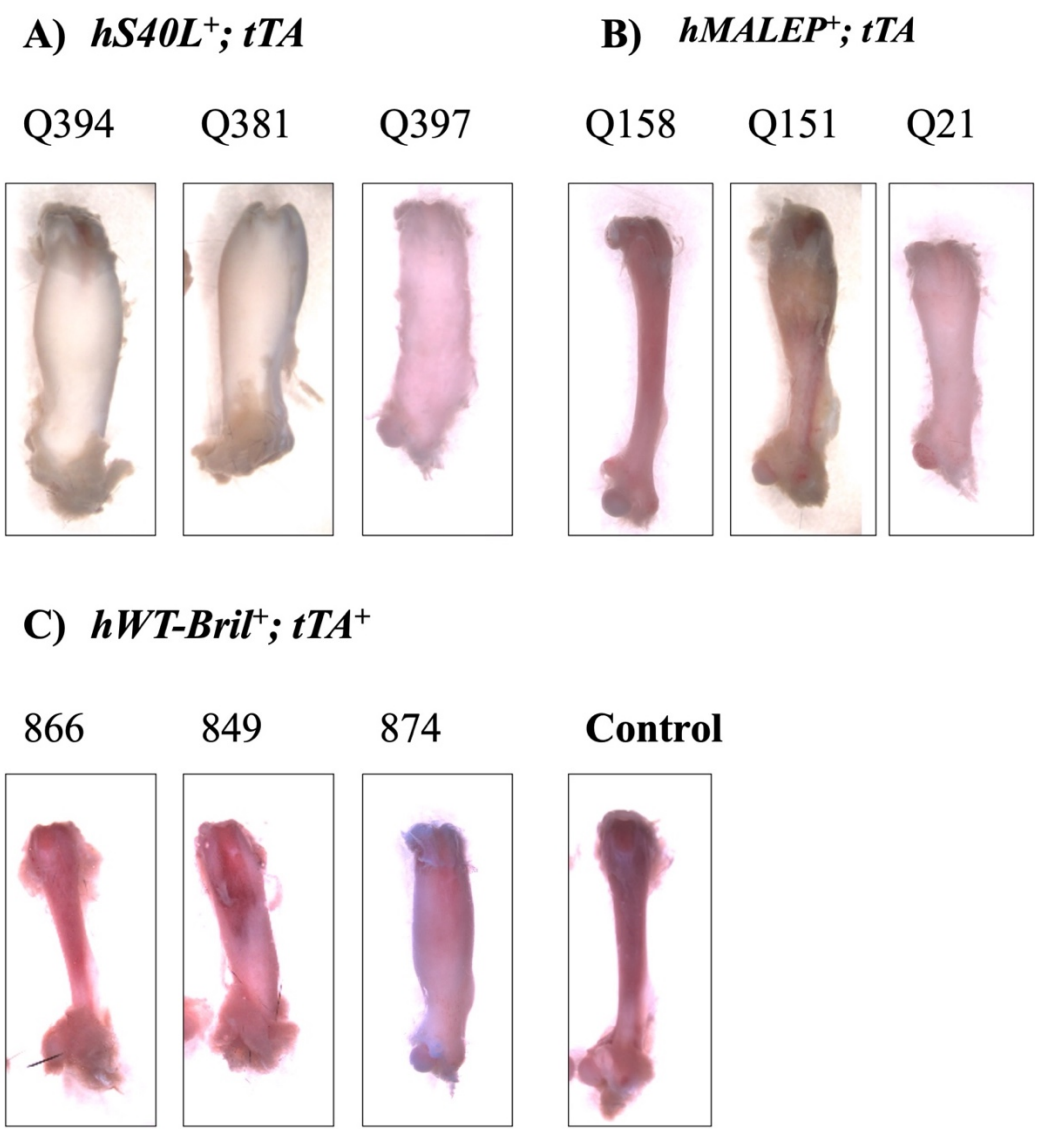

Figure 17: Representative images of femurs from mice expressing hS40L-BRIL, hMALEP-BRIL, and hWT-BRIL at 3 months of age.

A) Benchtop images of a representative femur for each hS40L line (Q394, Q381 and Q397).

B) Benchtop images of a representative femur for each hMALEP line (Q158, Q151, and Q21).

C) Benchtop images of a representative femur for each hWT-BRIL line (866, 849, and 874).

CHAPTER 4:DISCUSSION

The first goal of my project was to generate and characterize inducible transgenic mice expressing the BRIL variants hMALEP and hS40L. Unfortunately, at the onset of this project, the control mice expressing the wild type form of human BRIL (hWT-BRIL) had not been generated. These hWT-BRIL mice were extremely important as they represent the best control available to compare with the hMALEP-BRIL and hS40L-BRIL mice. They were obtained, however, only later once a substantial number of samples from the hMALEP and hS40L had been analyzed. Therefore, some of the results and conclusions drawn from the earlier analysis were rendered inconclusive, especially for the postnatal ages. Since the hWT-BRIL post-natal mice showed a similar bone overgrowth phenotype, the bone phenotype could not be attributed to the specific hS40L-BRIL or MALEP-BRIL mutations. This was disappointing as lots of effort, resources, and reagents had been put into the analyses, which did not lead to conclusive results. Nevertheless, we successfully obtained founder mice that did transmit the human BRIL transgene to the progeny. The descendants, whether embryos or adults allowed us to better understand the differences between them, and as such are still valuable for analysis.

When the transgenes were expressed constitutively (in the absence of Dox) under the regulation of the osterix promoter, both the hMALEP and hS40L-BRIL models displayed very similar embryonic phenotypes, leading to neo-natal lethality. The limbs and ribs of all mutant E18.5 embryos were bent and wavy. The extent of alizarin red staining in the limbs suggest that mineralization was significantly reduced. Further, the histological analysis of the humerus indicated that the midshaft was still cartilaginous with an enlarged hypertrophic zone where the midshaft and cortical bone would normally be present at that stage. The reduced expression of the BRIL protein in tissue extracts, at least in the hS40L, also pointed to a blunted

osteoblastogenesis process. In many ways, the phenotype of the two models was reminiscent of the previous OI type V (MALEP) knockin mouse model generated in our laboratory and others [49,50], which were also perinatal lethal. This is exemplified by the similar down regulation of *Bril*, *Ibsp*, and *Bglap*, but overexpression of *Ptgs2*. *Ptgs2* encodes the COX2 enzyme responsible for the synthesis of proinflammatory prostaglandins[59,60]. It is interesting to find similar upregulation of *Ptgs2* and possibly infer a commonality between the two models whereby inflammation may be involved, leading to a concomitant downregulation of these osteoblast-specific genes.

The severe skeletal manifestations observed for the hMALEP and hS40L mutants were never observed in the transgenic hWT-BRIL model at the embryonic or neonatal time points. All mice constitutively expressing the hWT-BRIL appeared normal at birth and all survive to adulthood, suggesting that the embryonic phenotype in the hMALEP and hS40L is specific for the mutant BRIL proteins. Another aspect that could have confounded the results and interpretation is the fact that the Osx-Cre driver mouse line has been shown previously to have some non-negligible skeletal anomalies[61,62] It is unlikely, however, that the phenotype observed in the embryos is due to the driver, as identical results were obtained (data not shown) when using another driver (Col1a1-tTA). Furthermore, the embryonic malformation and neo-natal lethality were visible in three independent lines for each of the hMALEP and hS40L models, thus excluding the possibility that the transgene expression levels, or transgene integration sites within the genome, were indirectly contributing. Because the phenotype of the two different models, for OI type V (hMALEP) and atypical type VI (hS40L) presented very similarly, they were not studied in more detail. It was decided instead to take another approach in order to determine possible differences between the two.

To gain further insight into what similar or distinct mechanisms maybe causing the skeletal phenotype in the hMALEP and hS40L, and halted osteoblastogenesis, neonatal calvarial osteoblast cultures were used. First, alizarin red staining at day 14 and 21 of cultures, showed that the hS40L had qualitatively less mineralization as compared to control and hMALEP and hWT cultures. Although the staining was not quantified, this reduction was repeatedly observed in the hS40L. The BRIL protein content showed even expression between the hS40L-BRIL, hMALEP-BRIL, and hWT-BRIL cultures, indicating all were being produced within the same kinetic time frame. Next, we decided to focus our attention on gene expression profiling using a given set of gene targets. The results indicated that the osteoblast differentiation markers *Bril, Alpl, Ibsp* and *Bglap* were all significantly repressed in the hS40L-BRIL cultures. Although the levels of gene expression of these genes in in the hMALEP cultures were repressed when compared to controls, they were nevertheless systematically higher than in the hS40L. Altogether these data indicated a more pronounced detrimental effect when the hS40L-BRIL is produced as compared to the hMALEP- BRIL. In both cases, the data also indicate that the phenotype is cell-autonomous. To further define potential effects of the hS40L in osteoblasts, other markers were analyzed. It had previously been observed that an osteoblast culture from an atypical type VI patient had decreased *SERPINF1* expression level, and paradoxically increased *COL1A1* levels[15]. Analysis of those two markers measured in our hS40L-BRIL osteoblasts showed that they were both reduced as compared to controls. Although the role of PEDF in skeletogenesis is still unclear, downregulation of *SerpinF1* and *Col1a1* in the primary hS40L osteoblasts would be consistent with the previous study. The results presented above appear to be contrasting with one study using primary osteoblast culture from OI type V patients[63]. In OI type V osteoblasts, Reich *et al*. reported that the extent of mineralization and the expression of bone markers (*Alpl*, *Ibsp*,

Bglap) were both increased[63]. However, in that study *Cola1a* gene expression was decreased in the mutant cells, as we have observed. It is at presently unclear why opposing alterations were observed. It may be speculated that culture conditions differences may have contributed to some extent, along with the use of BMP2 to drive the human osteoblast differentiation in the Reich study[63]. Also, osteoblasts from only one patient were examined. Thus, it is difficult to draw general conclusions where predicted variability between a control and one proband culture could have explained the differences. Our data with the hS40L-BRIL cultures align better with osteoblast cultures obtained from one atypical type VI patient as reported by Farber *et al*[15]. In that study, expression of *Alpl*, *Serpinf1* and *Col1a1* were significantly reduced in the hS40L patient osteoblasts as compared to control cultures. Thus, it appears that subtle differences are caused by the expression of the two mutant hMALEP and hS40L BRIL proteins.

Another possibility that we explored was based on the observation that adipose-like cells appeared in the hS40L cultures. This was validated by the trend towards increased expression, albeit variable, of *AdipoQ* and *Fabp4*. It is thus possible that the hS40L mutant induces a shift towards adipogenesis. Osteoblasts and adipocytes differentiate from a common precursor. Bone marrow contains pluripotent mesenchymal stem cells (MSCs) which can give rise to multiple different cell types including chondroblasts, adipocytes or osteoblasts[64]. This possible shift towards adipogenesis was unique to the hS40L-BRIL cultures and should be further studied with more replicate cultures and additional staining with Oil Red O as gene expression. It has also been reported that activated Wnt signalling promotes osteogenic differentiation [65]. In our post-natal hS40L-BRIL samples, RNAseq showed marked increases in Wnt inhibitors. Future experiments aimed at determining the expression levels of these Wnt inhibitors could be assayed in the neonatal osteoblast cultures.

Another aspect that could explain the more dramatic effect of the hS40L is related to its sub-cellular localization. *In vitro* immunofluorescence data from Patoine *et al* showed that the mouse hS42L-BRIL is trapped within the ER-Golgi network as is not localized properly at the plasma membrane[32]. We therefore hypothesized that the hS40L-BRIL protein could accumulate in the ER-Golgi network and cause a cellular stress response that could explain the higher negative effect on osteoblasts. Recently, endoplasmic reticulum (ER) stress has emerged as a common cellular pathologic process for several diseases, including OI. This has been documented in studies revolving around OI caused by defects in type I collagen or even in it its processing. Duran *et al* studied the use of 4-phenylbutiric acid (4-PBA), an established chemical chaperone in the treatment of Aga2+/- mice[66]. The Aga2+/- model is a model for moderately severe OI due to a structural mutation in Col1a1 structural mutation. 4-PBA treatment improved the phenotype[66]. Besio *et al* used cells from patients with OI types VII, VIII and IX, caused by recessive mutations in cartilage-associated protein (CRTAP), prolyl-3- hydroxylase 1 (P3H1) and cyclophilin B (PPIB), respectively[67]. All three types result in collagen that is over modified. These three proteins encode the components of the endoplasmic reticulum (ER) complex responsible for the 3-hydroxylation of specific proline residues of type I collagen[67]. They studied primary fibroblasts from seven recessive OI patients. In all cell lines, the intracellular retention of overmodified type I collagen molecules caused ER stress which was diminished using 4-PBA[67].

Given these examples of UPR activation being involved in OI, gene expression of key markers was assessed in the hS40L-BRIL osteoblast cultures. However, there was no consistent increase in these UPR markers seen in the hS40L-BRIL cultures over time when compared to control cultures past day 0 (confluency). The only significant differences observed were for the

Xbp1 and *Eif2ak3* (as well as a trend towards significance for *Atf4)*. These were increased at D0 in the hS40L-BRIL osteoblasts. *Xbp1* is part of the IRE1 pathway and *Atf4* and *Eif2ak3* are part of the PERK pathway. This would indicate that expression early in culture from seeding to confluence (day 0) would induce a cellular stress that did not further translate, for unknown reasons, at later time points. In another cellular context using the MC3T3-E1 osteoblast line, it was also investigated whether 4-PBA treatment of cells expressing the hS40L BRIL could prevent the protein from being trapped in the ER-Golgi (data not shown), but this was not the case. Although some differences in expression were observed in *Xbp1* and *Eif2ak3*, we cannot formally attribute the effect of hS40L to cellular stress as this was not consistent throughout the culture time-points.

As mentioned in the results section, expressing either hS40L-BRIL, hMALEP-BRIL, or hWT-BRIL led to a bone overgrowth phenotype and an increase in osteoblast activity markers. At least for the hMALEP and hS40L in which serum ALP was measured, both showed dramatically increased levels. ALP is normally a surrogate for bone formation and the elevated activity in the blood would indirectly corroborate the massive bone formation in the two mutant models[68]. Patients with atypical OI type VI have a severe form of OI and an increase in unmineralized osteoid seen in iliac bone histology using a Goldner stain[15]. Our post-natal hS40L-BRIL mice did now show the phenotype seen in the patients nor a consistent increase in unmineralized osteoid in their femur via Goldner staining[69,70]. Therefore, out post-natal mice did not fully recapitulate what is seen in the human aOI type VI patients[15]. However, both type of OI patients has been reported to display elevated serum ALP activity like we have observed in our model.

The RNASeq data from mice expressing hS40L-BRIL from 2-3 months does show important pathways have been affected (i.e., Wnt inhibition and inflammation) but it was not possible to determine what was the initial driver event and timing that caused the phenotype as it was far too progressed. At this stage, as there is already massive bone formation and dysregulation of gene expression. As for all cases of OI type V reported so far in the literature, the most consistent clinical manifestations are hyperplastic callus formation, radial head dislocation, and fractures. Our OI type V model did not recapitulate these clinical observations, as the constitutive expression of the human (present study) and previous mouse MALEP BRIL both led to a much more severe neo-natal lethality[49,50]. This is not the case in OI type V patients, as all patients survive to adulthood, and sometimes even have children of their own[10,12]. It should be mentioned that OI type V clinical manifestations are very variable: some patients do present with very severe symptoms, while others appear practically normal. The root cause for this variability is at present unknown, but it could be due to modifier genes, or genetic interactions, although this has not yet been tested.

Expressing hWT-BRIL post-natally unexpectedly resulted in a bone overgrowth phenotype that appears the same as the hMALEP-BRIL and hS40L-BRIL. This was very concerning and casting uncertainty to the post-natal phenotypic description presented above for the hMALEP-BRIL and hS40-BRIL. We can exclude the possibility that the phenotype produced by the hWT-BRIL is simply due to excessive overexpression of the protein in that particular model. In fact, a comparison of the expression of the human BRIL transgene in all three models and across all three lines for each revealed similar levels. However, ongoing work in our laboratory would indicate that the wild-type human BRIL protein could possess anabolic properties when overexpressed in mice. This interpretation is based on data showing that

overexpression of the mouse BRIL protein in transgenic mice did not cause such massive bone accrual when put under the regulation of the *Col1a1* promoter[48,71]. Expression of the mouse wild-type BRIL using the same backbone (Tet-off) as that described in the current study also did not yield any significant post-natal bone expansion (data not shown). These data would suggest that subtle differences in the amino acid composition between the human and mouse BRIL protein could drive this effect. When mouse and human BRIL protein sequences are compared, they display 78% identity (105/134 exact same amino acid) and 91% similarity (122/134 conserved amino acid)[28]. Only 10 amino acid residues are dissimilar between the two proteins, and future studies could be set up to determine which of these residues are causing the human-specific phenotype. If feasible and conclusive, this type of study could ultimately lead to developing peptides that might be anabolic to bone and could be used therapeutically. As a starting point, site-directed mutagenesis of the mouse protein having humanized sequences could be explored to test this possibility *in vitro* in the MC3T3 cell lines.

Despite all the caveats discussed above, the post-natal experiments did present some differences between the hMALEP and hS40L models. Firstly, the localization of the hS40L-BRIL protein being produced *in vivo* which seemed to be reminiscent of the ER-Golgi localization detected *in vitro*. The high magnification pictures shown for the immunohistochemical detection of human BRIL tend to suggest a more discrete and localized punctate signal, as opposed to the cell-membrane visualization of the hMALEP-BRIL and hWT BRIL. However, further confirmation of this intracellular signal for the hS40L-BRIL would need to be obtained by doing co-immunostaining on the tissue sections with ER-Golgi specific markers such as HSP40 and Giantin. This would show that the hS40L protein is retained intracellularly *in vivo*. Secondly, only the hS40L-BRIL mice showed a significant decrease in

BUN. Urea is the primary metabolite derived from dietary protein and tissue protein turnover that occurs in the liver. Lower blood BUN levels can be associated with different physiological conditions such as liver dysfunction, but also with low-protein diet and malnutrition. This reflects a global decrease in protein synthesis[72]. In the case of the hS40L-BRIL mice, the reduction observed is unlikely caused by liver dysfunction as the hS40L-BRIL is not expressed in liver tissue. A more likely possibility would be the inability of the mice to eat adequately. The jaw bones (mandibles and maxilla) in the hS40L mice were also affected by the bone expansion. This could have caused mastication and/or temporomandibular joint problems leading to reduced food consumption. This could be proven by measuring the food uptake (was not done in this study). Interestingly, the jaw bone problems were also visible in the hMALEP-BRIL model, but this was not coupled with lower BUN levels. This could indicate a more profound phenotype-specific effect in the hS40L-BRIL.

CHAPTER 5:CONCLUSIONS

Overall, humanized inducible transgenic models have been generated and characterized for hS40L-BRIL (aOI type VI) and hMALEP-BRIL (OI type V). At the embryonic stage, we confirm that expression of either of these mutant forms of BRIL leads to severe skeletal defects and perinatal lethality. Calvarial osteoblast cultures for each of these models confirm that this arrest in osteoblastogenesis and resulting hypomineralization is cell autonomous. No significant upregulation of UPR markers was observed in hS40L-BRIL cultures over time, as compared to controls. However, significant increases in *Xbp1* (p value=0.0061) and *Eif2k3* (p value=0.0015) in hS40L cultures were observed at D0. This could indicate an initial UPR which did not continue over the course of the culture. Observations leading to additional mechanistic possibilities were discussed in chapter 4. These models could be employed as OI mouse models at the embryonic stage. In fact, the embryonic hMALEP-BRIl phenotype was consistent with the type V knockin model from our laboratory[49].

Post-natal expression of hS40L-BRIL or hMALEP-BRIL resulted in trabecular bone expansion into the periosteal compartment. This was correlated with an increase in osteoblast cell activity and differentiation markers. Serum ALPL was increased in both hMALEP and hS40L mice at 3 months of age. The post-natal phenotype does not replicate what is seen in the type V or atypical OI type VI patients. Thus overall, we were unsuccessful in generating an animal model that accurately mimicked OI type V post-natally. Thus, these models could not be used to study OI type V or VI in terms of growth or aging. Unfortunately, the majority of the hMALEP-BRIL and hS40L-BRIL post-natal samples were collected and analyzed before the generation of the hWT-BRIl model. Since the hWT-BRIL showed a similar bone accrual

phenotype when expressed post-natally, this suggests that the observed phenotype is caused by hBRIL. Since only10 amino acid residues are dissimilar between the two proteins, future studies could be geared towards determining which of these residues are causing the human-specific phenotype. If successful, this research could lead to a peptide with an anabolic effect in bone with potential therapeutic benefit.

CHAPTER 6:REFERENCES

1 Jovanovic, M., Guterman-Ram, G. & Marini, J. C. Osteogenesis imperfecta: mechanisms and signaling pathways connecting classical and rare OI types. *Endocrine reviews* **43**, 61-90 (2022).

2 Sillence, D. & Rimoin, D. Classification of osteogenesis imperfecta. *The Lancet* **311**, 1041-1042 (1978).

3 Sillence, D., Senn, A. & Danks, D. Genetic heterogeneity in osteogenesis imperfecta. *Journal of medical genetics* **16**, 101-116 (1979).

4 Forlino, A. & Marini, J. C. Osteogenesis imperfecta. *The Lancet* **387**, 1657-1671 (2016).

5 Marini, J. C., Reich, A. & Smith, S. M. Osteogenesis Imperfecta due to Mutations in Non-Collagenous Genes-Lessons in the Biology of Bone Formation. *Current opinion in pediatrics* **26**, 500 (2014).

6 Mortier, G. R. *et al.* Nosology and classification of genetic skeletal disorders: 2019 revision. *American Journal of Medical Genetics Part A* **179**, 2393-2419 (2019).

7 Glorieux, F. H. *et al.* Type V osteogenesis imperfecta: a new form of brittle bone disease. *Journal of Bone and Mineral Research* **15**, 1650-1658 (2000).

8 Semler, O. *et al.* A mutation in the 5′-UTR of IFITM5 creates an in-frame start codon and causes autosomal-dominant osteogenesis imperfecta type V with hyperplastic callus. *The American Journal of Human Genetics* **91**, 349-357 (2012).

9 Cho, T.-J. *et al.* A single recurrent mutation in the 5′-UTR of IFITM5 causes osteogenesis imperfecta type V. *The American Journal of Human Genetics* **91**, 343-348 (2012).

10 Rauch, F. *et al.* Osteogenesis imperfecta type V: marked phenotypic variability despite the presence of the IFITM5 c.− 14C> T mutation in all patients. *Journal of medical genetics* **50**, 21-24 (2013).

11 Cao, Y.-J., Wei, Z., Zhang, H. & Zhang, Z.-L. Expanding the clinical spectrum of osteogenesis imperfecta type V: 13 additional patients and review. *Frontiers in Endocrinology* **10**, 375 (2019).

12 Zhytnik, L. *et al.* IFITM5 pathogenic variant causes osteogenesis imperfecta V with various phenotype severity in Ukrainian and Vietnamese patients. *Human genomics* **13**, 1-11 (2019).

13 Retrouvey, J.-M. *et al.* Oro-dental and cranio-facial characteristics of osteogenesis imperfecta type V. *European journal of medical genetics* **62**, 103606 (2019).

14 Lazarus, S. *et al.* The IFITM5 mutation c.-14C> T results in an elongated transcript expressed in human bone; and causes varying phenotypic severity of osteogenesis imperfecta type V. *BMC musculoskeletal disorders* **15**, 1-6 (2014).

15 Farber, C. R. *et al.* A Novel IFITM5 Mutation in Severe Atypical Osteogenesis Imperfecta Type VI Impairs Osteoblast Production of Pigment Epithelium-Derived Factor. *Journal of Bone and Mineral Research* **29**, 1402-1411 (2014).

16 Hoyer-Kuhn, H. *et al.* A nonclassical IFITM5 mutation located in the coding region causes severe osteogenesis imperfecta with prenatal onset. *Journal of Bone and Mineral Research* **29**, 1387-1391 (2014).

17 Rodriguez Celin, M., Moosa, S. & Fano, V. Uncommon IFITM5 mutation associated with severe skeletal deformity in osteogenesis imperfecta. *Annals of Human Genetics* **82**, 477-481 (2018).

18 Lim, J. Y. *et al.* A novel Ser40Trp variant in IFITM5 in a family with osteogenesis imperfecta and review of the literature. *Clinical Dysmorphology* **28**, 118-123 (2019).

19 Glorieux, F. H. *et al.* Osteogenesis imperfecta type VI: a form of brittle bone disease with a mineralization defect. *Journal of Bone and Mineral Research* **17**, 30-38 (2002).

20 Homan, E. P. *et al.* Mutations in SERPINF1 cause osteogenesis imperfecta type VI. *Journal of Bone and Mineral Research* **26**, 2798-2803 (2011).

21 Venturi, G. *et al.* Lack of expression of SERPINF1, the gene coding for pigment epithelium-derived factor, causes progressively deforming osteogenesis imperfecta with normal type I collagen. *Journal of Bone and Mineral Research* **27**, 723-728 (2012).

22 Becerra, S. P. & Notario, V. The effects of PEDF on cancer biology: mechanisms of action and therapeutic potential. *Nature Reviews Cancer* **13**, 258-271 (2013).

23 Marciniak, K., Butwicka, A. & Nowak, J. Z. PEDF: an endogenous factor displaying potent neuroprotective, neurotrophic, and antiangiogenic activity. *Postepy higieny i medycyny doswiadczalnej (Online)* **60**, 387-396 (2006).

24 Dawson, D. *et al.* Pigment epithelium-derived factor: a potent inhibitor of angiogenesis. *Science* **285**, 245-248 (1999).

25 Rauch, F., Husseini, A., Roughley, P., Glorieux, F. H. & Moffatt, P. Lack of circulating pigment epithelium-derived factor is a marker of osteogenesis imperfecta type VI. *The Journal of Clinical Endocrinology & Metabolism* **97**, E1550-E1556 (2012).

26 Mäkitie, R. *et al.* A Novel IFITM5 Variant Associated with Phenotype of Osteoporosis with Calvarial Doughnut Lesions: A Case Report. *Calcified tissue international* **109**, 626-632 (2021).

27 Wu, D., Wang, Y. & Huang, H. A novel variant of the IFITM5 gene within the 5′-UTR causes neonatal transverse clavicular fracture: Expanding the genetic spectrum. *Molecular Genetics & Genomic Medicine* **8**, e1287 (2020).

28 Moffatt, P. *et al.* Bril: a novel bone-specific modulator of mineralization. *Journal of Bone and Mineral Research* **23**, 1497-1508 (2008).

29 Hanagata, N., Takemura, T., Monkawa, A., Ikoma, T. & Tanaka, J. Phenotype and gene expression pattern of osteoblast-like cells cultured on polystyrene and hydroxyapatite with pre-adsorbed type-I collagen. *Journal of Biomedical Materials Research Part A: An Official Journal of The Society for Biomaterials, The Japanese Society for Biomaterials, and The Australian Society for Biomaterials and the Korean Society for Biomaterials* **83**, 362-371 (2007).

30 Hickford, D., Frankenberg, S., Shaw, G. & Renfree, M. B. Evolution of vertebrate interferon inducible transmembrane proteins. *BMC genomics* **13**, 1-11 (2012).

31 Friedman, R. L., Manly, S. P., McMahon, M., Kerr, I. M. & Stark, G. R. Transcriptional and posttranscriptional regulation of interferon-induced gene expression in human cells. *Cell* **38**, 745-755 (1984).

32 Patoine, A. *et al.* Topological mapping of BRIL reveals a type II orientation and effects of osteogenesis imperfecta mutations on its cellular destination. *Journal of Bone and Mineral Research* **29**, 2004-2016 (2014).

33 Siegrist, F., Ebeling, M. & Certa, U. The small interferon-induced transmembrane genes and proteins. *Journal of Interferon & Cytokine Research* **31**, 183-197 (2011).

34 Huang, I.-C. *et al.* Distinct patterns of IFITM-mediated restriction of filoviruses, SARS coronavirus, and influenza A virus. *PLoS pathogens* **7**, e1001258 (2011).

35 Lu, J., Pan, Q., Rong, L., Liu, S.-L. & Liang, C. The IFITM proteins inhibit HIV-1 infection. *Journal of virology* **85**, 2126-2137 (2011).

36 Brass, A. L. *et al.* The IFITM proteins mediate cellular resistance to influenza A H1N1 virus, West Nile virus, and dengue virus. *Cell* **139**, 1243-1254 (2009).

37 Kasaai, B., Gaumond, M.-H. & Moffatt, P. Regulation of the bone-restricted IFITM-like (Bril) gene transcription by Sp and Gli family members and CpG methylation. *Journal of Biological Chemistry* **288**, 13278-13294 (2013).

38 Robbins, D. J., Fei, D. L. & Riobo, N. A. The Hedgehog signal transduction network. *Science signaling* **5**, re6-re6 (2012).

39 Corradi, M. *et al.* The recurrent causal mutation for osteogenesis imperfecta type V occurs at a highly methylated CpG dinucleotide within the IFITM5 gene. *Journal of Pediatric Genetics* **3**, 035-039 (2014).

40 Weston, S. *et al.* A membrane topology model for human interferon inducible transmembrane protein 1. *PloS one* **9**, e104341 (2014).

41 Bailey, C. C., Kondur, H. R., Huang, I.-C. & Farzan, M. Interferon-induced transmembrane protein 3 is a type II transmembrane protein. *Journal of Biological Chemistry* **288**, 32184-32193 (2013).

42 Philippe, J. M. & Jenkins, P. M. Spatial organization of palmitoyl acyl transferases governs substrate localization and function. *Molecular membrane biology* **35**, 60-75 (2019).

43 Tsukamoto, T. *et al.* Role of S-palmitoylation on IFITM5 for the interaction with FKBP11 in osteoblast cells. *Plos one* **8**, e75831 (2013).

44 Hanagata, N. & Li, X. Osteoblast-enriched membrane protein IFITM5 regulates the association of CD9 with an FKBP11–CD81–FPRP complex and stimulates expression of interferon-induced genes. *Biochemical and biophysical research communications* **409**, 378-384 (2011).

45 Maranda, V., Gaumond, M.-H. & Moffatt, P. The Osteogenesis Imperfecta Type V Mutant BRIL/IFITM5 Promotes Transcriptional Activation of MEF2, NFATc, and NR4A in Osteoblasts. *International Journal of Molecular Sciences* **23**, 2148 (2022).

46 Hanagata, N. *et al.* Characterization of the osteoblast-specific transmembrane protein IFITM5 and analysis of IFITM5-deficient mice. *Journal of bone and mineral metabolism* **29**, 279-290 (2011).

47 Patoine, A., Husseini, A., Kasaai, B., Gaumond, M.-H. & Moffatt, P. The osteogenic cell surface marker BRIL/IFITM5 is dispensable for bone development and homeostasis in mice. *PloS one* **12**, e0184568 (2017).

48 Lietman, C. D. *et al.* A transgenic mouse model of OI type V supports a neomorphic mechanism of the IFITM5 mutation. *Journal of Bone and Mineral Research* **30**, 489-498 (2015).

49 Rauch, F. *et al.* Crispr-Cas9 engineered osteogenesis imperfecta type V leads to severe skeletal deformities and perinatal lethality in mice. *Bone* **107**, 131-142 (2018).

50 Hanagata, N., Takemura, T., Kamimura, K. & Koda, T. Effect of immunosuppressants on a mouse model of osteogenesis imperfecta type V harboring a heterozygous Ifitm5 c.-14C> T mutation. *Scientific reports* **10**, 1-11 (2020).

51 Hanagata, N. IFITM5 mutations and osteogenesis imperfecta. *Journal of bone and mineral metabolism* **34**, 123-131 (2016).

52 Hedjazi, G. *et al.* Alterations of bone material properties in growing Ifitm5/BRIL p. S42 knock-in mice, a new model for atypical type VI osteogenesis imperfecta. *Bone*, 116451 (2022).

53 Rodda, S. J. & McMahon, A. P. Distinct roles for Hedgehog and canonical Wnt signaling in specification, differentiation and maintenance of osteoblast progenitors. *Development* **133**, 3231-3244 (2006).

54 Peng, J. *et al.* Conditional expression of a Gi-coupled receptor in osteoblasts results in trabecular osteopenia. *Endocrinology* **149**, 1329-1337 (2007).

55 McLeod, M. J. Differential staining of cartilage and bone in whole mouse fetuses by alcian blue and alizarin red S. *Teratology* **22**, 299-301 (1980).

56 Hekmatnejad, B., Vionnie, W., Akhouayri, O., Arabian, A. & St-Arnaud, R. Altered gene dosage confirms the genetic interaction between FIAT and αNAC. *Gene* **538**, 328-333 (2014).

57 Walter, P. & Ron, D. The unfolded protein response: from stress pathway to homeostatic regulation. *science* **334**, 1081-1086 (2011).

58 Mortazavi, A., Williams, B. A., McCue, K., Schaeffer, L. & Wold, B. Mapping and quantifying mammalian transcriptomes by RNA-Seq. *Nature methods* **5**, 621-628 (2008).

59 Blackwell, K. A., Raisz, L. G. & Pilbeam, C. C. Prostaglandins in bone: bad cop, good cop? *Trends in Endocrinology & Metabolism* **21**, 294-301 (2010).

60 Zhang, X. *et al.* Cyclooxygenase-2 regulates mesenchymal cell differentiation into the osteoblast lineage and is critically involved in bone repair. *The Journal of clinical investigation* **109**, 1405-1415 (2002).

61 Wang, L., Mishina, Y. & Liu, F. Osterix-Cre transgene causes craniofacial bone development defect. *Calcified tissue international* **96**, 129-137 (2015).

62 Davey, R. A. *et al.* Decreased body weight in young Osterix-Cre transgenic mice results in delayed cortical bone expansion and accrual. *Transgenic research* **21**, 885-893 (2012).

63 Reich, A. *et al.* Type V OI primary osteoblasts display increased mineralization despite decreased COL1A1 expression. *The Journal of Clinical Endocrinology & Metabolism* **100**, E325-E332 (2015).

64 Almalki, S. G. & Agrawal, D. K. Key transcription factors in the differentiation of mesenchymal stem cells. *Differentiation* **92**, 41-51 (2016).

65 Cawthorn, W. P. *et al.* Wnt6, Wnt10a and Wnt10b inhibit adipogenesis and stimulate osteoblastogenesis through a β-catenin-dependent mechanism. *Bone* **50**, 477-489 (2012).

66 Duran, I. *et al.* 4-PBA treatment improves bone phenotypes in the Aga2 mouse model of osteogenesis imperfecta. *Journal of Bone and Mineral Research* (2022).

67 Besio, R. *et al.* Cellular stress due to impairment of collagen prolyl hydroxylation complex is rescued by the chaperone 4-phenylbutyrate. *Disease models & mechanisms* **12**, dmm038521 (2019).

68 Linder, C. H., Englund, U. H., Narisawa, S., Millán, J. L. & Magnusson, P. Isozyme profile and tissue-origin of alkaline phosphatases in mouse serum. *Bone* **53**, 399-408 (2013).

69 Villanueva, A. R. A new Goldner's one-step trichrome stain for identification of osteoid seams, bone and cells in undecalcified, plastic embedded sections of bone. *Journal of Histotechnology* **11**, 249-251 (1988).

70 Ralis, Z. & Watkins, G. Modified tetrachrome method for osteoid and defectively mineralized bone in paraffin sections. *Biotechnic & histochemistry* **67**, 339-345 (1992).

71 Patoine, A. *Characterization of a transgenic mouse overexpressing the osteogenesis imperfecta type V mutant BRIL*. (McGill University (Canada), 2015).

72 Hosten, A. O. BUN and Creatinine. *Clinical Methods: The History, Physical, and Laboratory Examinations. 3rd edition* (1990).

CHAPTER 7:SUPPLEMENTARY DATA

November 5, 2021 (Amended December 7, 2021)

Amended Animal Certificate

This is to certify that **Prof. Pierre Moffatt, Department of Human Genetics, Shriners Hospital,** currently holds an approved **Animal Use Protocol # 2012-7235** with McGill University and its Affiliated Hospital's Research Institutes for the following project:

Animal Use Protocol Title: The role of BRIL in the pathogenesis of osteogenesis imperfecta. / Exploring the role of Msmp in the skeleton / A translational approach to treat osteogenesis imperfecta type V: proof of principle

Start date: October 1, 2021

Expiration date: September 30, 2022

McGill University and Affiliated Hospitals Research Institutes recognize the importance of animal research in our efforts to further our knowledge of natural processes, diseases and conservation. Research, educational and testing projects are conducted with full commitment to the wellbeing of the animal subjects. In order to limit animal use to meritorious research or educational projects, the institution relies on stringent peer review processes, along with assessment of ethical issues by the Animal Care Committee. McGill University recognizes that the use of animals in research, teaching and testing carries significant responsibilities. The institution will continue to develop and maintain guidelines and regulations, following the high standards established by the Canadian Council on Animal Care. It is committed to conducting the highest-quality research and to providing animals with the best care.

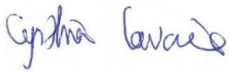

Cynthia Lavoie
Animal Ethics and Compliance Administrator
Animal Compliance Office
Office of Vice-Principal (Research and Innovation)
Suite 325, James Administration Building, McGill University
845 Sherbrooke Street West, Montreal, Quebec, Canada H3A 0G4
animal.approvals@mcgill.ca

Supplementary Figure 1: Animal Use Certificate

Animal use certificate issued by the Animal Ethics and Compliance Administrator. This protocol was used for this project.